The MiMeS survey of magnetism in massive stars: magnetic properties of the O-type star population

V. Petit, G. A. Wade, F. R. N. Schneider, L. Fossati, K. Kamp, Coralie Neiner, A. David-Uraz, E. Alecian, The Mimes Collaboration

Monthly Notices
of the
ROYAL ASTRONOMICAL SOCIETY

MNRAS **489,** 5669–5687 (2019)
Advance Access publication 2019 September 11

doi:10.1093/mnras/stz2469

The MiMeS survey of magnetism in massive stars: magnetic properties of the O-type star population

V. Petit [1]★ G. A. Wade,[2] F. R. N. Schneider,[3,4] L. Fossati,[5] K. Kamp,[6] C. Neiner [7] A. David-Uraz [1] and E. Alecian[8]

(the MiMeS Collaboration)

[1]*Department of Physics & Astronomy, University of Delaware, Newark, DE 19716, USA*
[2]*Department of Physics & Space Science, Royal Military College of Canada, PO Box 17000, Kingston, ON K7K 7B4, Canada*
[3]*Zentrum für Astronomie der Universität Heidelberg, Astronomisches Rechen-Institut, Mönchhofstr 12–14, D-69120 Heidelberg, Germany*
[4]*Heidelberger Institut für Theoretische Studien, Schloss-Wolfsbrunnenweg 35, D-69118 Heidelberg, Germany*
[5]*Space Research Institute, Austrian Academy of Sciences, Schmiedlstrasse 6, A-8042 Graz, Austria*
[6]*Department of Aerospace, Physics and Space Sciences, Florida Institute of Technology, 150 W. University Blvd, Melbourne, FL 32901, USA*
[7]*LESIA, Paris Observatory, PSL University, CNRS, Sorbonne Université, Université de Paris, 5 place Jules Janssen, F-92195 Meudon, France*
[8]*Université Grenoble Alpes, CNRS, IPAG, F-38000 Grenoble, France*

Accepted 2019 September 2. Received 2019 August 23; in original form 2019 June 15

ABSTRACT

In this paper, we describe an analysis of the MiMeS (Magnetism in Massive Stars) survey of O-type stars to explore the range of dipolar field strengths permitted by the polarization spectra that do not yield a magnetic detection. We directly model the Stokes *V* profiles with a dipolar topology model using Bayesian inference. The noise statistics of the Stokes *V* profiles are in excellent agreement with those of the null profiles. Using a Monte Carlo approach, we conclude that a model in which all the stars in our sample were to host 100 G, dipolar magnetic field can be ruled out by the MiMeS data. Furthermore, if all the stars with no detection were to host a magnetic field just below their detection limit, the inferred distribution in strength of these undetected fields would be distinct from the known distribution in strength of the known magnetic O-type stars. This indicates that the 'initial magnetic field function' (IBF) is likely bimodal – young O-type stars are expected to have either weak/absent magnetic fields or strong magnetic fields. We also find that better upper limits, by at least a factor of 10, would have been necessary to rule out a detection bias as an explanation for the apparent lack of evolved main-sequence magnetic O-type stars reported in the literature, and we conclude that the MiMeS survey cannot confirm or refute a magnetic flux decay in O-type stars.

Key words: stars: early-type – stars: magnetic field – stars: massive.

1 MOTIVATION AND GOALS

Magnetic fields are now routinely detected at the surfaces of a subsample of OB stars. These fields generally have a simple, mostly dipolar topology. They are also strong, with dipolar strength values ranging from a few hundred gauss to tens of kilogauss (e.g. Petit et al. 2013; Shultz et al. 2018). Their rarity, along with the lack of observed short-term (days to decades) evolution, suggests that these fields are not generated by a contemporaneous dynamo mechanism, as is the case for solar-type stars, but are rather a relic from an event or an evolutionary phase that occurred earlier in their past (e.g. Borra, Landstreet & Mestel 1982).

These so-called fossil fields are now increasingly well characterized, thanks to the advent of large surveys performed with high-resolution spectropolarimetric instrumentation (e.g. Fossati et al. 2015; Wade et al. 2016). These instruments allow for the measurement of the polarization change across spectral lines introduced by the Zeeman effect (for an in-depth review, see Donati & Landstreet 2009).

This paper constitutes the second part of the study initiated by Grunhut et al. (2017, hereafter Paper I) that characterized the 97 O-type star systems observed with spectropolarimetry within the context of the MiMeS (Magnetism in Massive Stars) survey. The MiMeS survey was performed through Large Program allocations with the high-resolution spectrographs ESPaDOnS at the Canada–France–Hawaii Telescope, Narval at the Télescope Bernard Lyot in France, and HARPSpol at the ESO La Silla 3.6 m in Chile (Wade et al. 2016).

Paper I presented the detection statistics for the survey based on the presence of a polarization signal in Stokes *V*, and on the

★ E-mail: VPetit@UDel.edu

associated measurement of the surface-averaged longitudinal field B_l that represents the component of the magnetic field along the line of sight, integrated over the stellar disc (thus weighted by the local intensity).

Among the main results, Paper I reported that

(i) the median MiMeS survey precision for the longitudinal field is 50 G;
(ii) the detection of six new magnetic O-type stars implies a magnetic incidence fraction of 7 ± 3 per cent; in addition, marginal signal was detected in three stars that were therefore deemed to be magnetic candidates;
(iii) there are no correlations between the presence of a magnetic field and any stellar parameters of the sample (other than the expected slow bulk rotation);
(iv) there is a direct link between the so-called Of?p spectral peculiarities (Walborn 1972) and magnetism, although not all magnetic O-type stars have these peculiarities.

In this paper, we perform an analysis of the O-type stars without a magnetic field detection to explore the dipolar field strengths permitted by the polarization spectra. We directly model the Stokes V profiles with the Bayesian inference procedure developed by Petit & Wade (2012) for a dipolar field topology.

Such a study allows us to address several questions concerning the distribution of magnetic fields in O-type stars, described in the following two sections. It also provides an independent evaluation of the polarization signature of the magnetic candidate stars, as well as the potential to identify additional magnetic candidates.

1.1 Is there a magnetic desert for O-type stars?

In magnetic A-type stars, there is a known deficit of stars with dipole field strengths at the ∼100 G level (Aurière et al. 2007). This so-called magnetic desert (Lignières et al. 2014) is a well-established result for a few reasons:

(i) It has been long established that strong magnetism and the Ap-type chemical peculiarities are linked (Aurière et al. 2007), making strongly magnetic A-type stars easily identifiable through spectroscopic peculiarities and photometric/spectroscopic variations due to abundance spots.
(ii) The field detection limits for A-type stars are generally very good, due to the multitude and sharpness of their metallic spectral features. This has been recently exemplified by the detection of very weak (at the sub-gauss level) magnetic fields at the surface of some A-type stars (Petit et al. 2010, 2011; Blazère et al. 2016). Clearly, significantly stronger fields would have been noticed – nevertheless, there are only a handful of known main-sequence magnetic A-type stars in the 1–100 G field strength bin (Alecian et al. 2016; Blazère et al. 2018).

Is there an extension of the 'magnetic desert' phenomenon for the O-type stars? Using our sample we determine whether the detection limits obtained for O-type stars are sufficient to establish the existence of a magnetic desert in the O-type stars.

1.2 Can we detect magnetic fields in old main-sequence O-type stars, and thereby constrain models of the evolution of their surface magnetism?

An interesting additional application for this sample of upper limits on dipolar field strength is to explore the cause of the apparent scarcity of evolved (hereafter referred to as 'old') massive stars (near or past the terminal-age maine sequence (TAMS))) with a detected magnetic field (Fossati et al. 2016, hereafter F2016). F2016 compared the age distribution of the known magnetic OB stars with that of a magnitude-limited comparison sample of OB stars. These ages were derived using the Bayesian tool BONNSAI (Schneider et al. 2014, 2017), using the evolution tracks of Brott et al. (2011). F2016 found that, in general, the main-sequence fractional ages of the magnetic OB stars are smaller than those of their non-magnetic counterparts, and possibly even more so for stars with higher zero-age main-sequence (ZAMS) masses.

F2016 discuss three possible physical explanations for this result:

(i) The magnetic fields at the surfaces of these stars may decrease more quickly than expected from the magnetic flux conservation hypothesis (the reduction of surface field coming from flux freezing combined with the evolutionary increase in radius; Landstreet et al. 2008), implying a loss of magnetic flux by, for example, Ohmic decay.
(ii) Magnetic stars could appear younger than they really are when their ages are estimated using non-magnetic evolutionary models, due to the suppression of convective core overshoot (Briquet et al. 2012). F2016 suggest that in this example case, one would expect an inverse correlation between inferred young apparent age and field strength, which was not observed in their study. We note here that other processes involving the interaction between surface magnetic fields and mass-loss (such as magnetic braking and mass-loss quenching) have also been shown to have marked but complex evolutionary effects that should be taken into account when estimating evolutionary ages, especially for more massive stars (Maeder & Meynet 2005; Georgy et al. 2017; Petit et al. 2017; Keszthelyi et al. 2019).
(iii) Finally, one proposed pathway for the generation of fossil magnetic fields is via binary mergers (e.g. Schneider et al. 2016). The rejuvenation of the merger product could lead to a seemingly younger magnetic population. However, F2016 argue that in a scenario of constant star formation history, the population of mass gainers will be biased towards larger fractional main sequence (MS) age.

Importantly, F2016 also point out some possible observational biases that could result in the inferred age distribution for known magnetic stars. They performed a preliminary assessment of the magnetic detection limits, based on the field strengths of the weakest known magnetic OB stars as a function of V magnitude. Their estimate suggested that some of the known magnetic stars would still be detectable with current instrumentation upon reaching their TAMS. As a consequence, observational bias was not considered by those authors to be a likely explanation for the apparent lack of old magnetic OB stars. However, this assessment of observational bias does not take into account the characteristics of the typical spectropolarimetric survey – some of the known magnetic stars were first identified by other means (e.g. indirect magnetospheric emission/variation), and may have been observed with deeper detection limits than those of the typical large survey.

With the MiMeS O-star sample, we can directly address the observational biases, for O-type stars, by answering the following two questions:

(i) Has a sufficiently large sample of old MS O-stars been searched for surface magnetic fields?

Table 1. List of the magnetic O-type stars considered in the study of F2016, with the field strength values as well as the current-day, ZAMS, and TAMS radii determined by F2016 and used in Section 5.1.2.

Star	$B_{\rm pole}$ (kG)	$\tau_{\rm MS}$	$R_{\rm current}$ ($R_\odot$)	$R_{\rm ZAMS}$ ($R_\odot$)	$R_{\rm TAMS}$ ($R_\odot$)
(1)	(2)	(3)	(4)	(5)	(6)
HD 148937	1.0	0.4	9.00	7.41	95.3
HD 37022	1.1	0.1	7.19	6.72	48.9
HD 191612	2.5	0.65	11.6	7.08	69.2
HD 47129	2.8	0.4	6.30	5.25	22.4
HD 108	0.5	0.69	13.17	7.39	93.1
HD 57682	1.7	0.53	7.43	5.81	29.0
HD 54879	2.0	0.48	6.88	5.4	23.6

(ii) If so, were the detection limits sufficiently precise to inform models of the evolution of their surface magnetism?

1.3 Paper structure

The paper is structured in the following way. In Section 2, we briefly summarize the observations. In Section 3, we summarize the application of the Bayesian technique of Petit & Wade (2012) to our sample, including the way in which we treat spectroscopic binary systems. In Section 4, we present the statistical properties of our sample of magnetic field upper limits. In Section 5, we interpret our results in the context of (i) evaluating the presence of a magnetic desert in magnetic O-type stars and (ii) explaining the apparent lack of old, main-sequence magnetic massive stars. We finally summarize our findings in Section 6.

2 OBSERVATIONS

The spectropolarimetric observations used here and in Paper I were obtained in the larger context of the MiMeS survey, described by Wade et al. (2016). To summarize, high-resolution echelle spectropolarimetric observations enable the measurement of the change in polarization across spectral lines induced by the Zeeman effect.

The sample of Paper I consists of 432 nightly averaged Stokes V observations of 97 O-type stars. Our sample here consists of stars without definite magnetic detection, reducing it to the 91 stars listed in Table 2 (which additionally contains the 11 O-type secondary stars in the SB2/SB3 system discussed in Section 3.1). Column 1 provides an identification number for easy reference, column 2 the HD number or BD number, and column 3 the spectral type.

In Paper I, the least-squares deconvolution (LSD) method (Donati et al. 1997) was used to produce a high signal-to-noise, mean line profile from each nightly averaged observation. The underlying principle of this method is that in the limit where the Zeeman splitting has a minimal impact on the intensity line profile (the so-called weak-field approximation; Landi degl'Innocenti & Landolfi 2004), the shape of the Stokes V profile remains the same from line to line, with an amplitude scaled by the wavelength and effective Landé factor of the electronic transition. We use these same LSD profiles here. Within the detection limits obtained in our results, the weak-field approximation is always valid. Column 4 of Table 2 gives the number of nightly averaged observations per star.

In Paper I, each nightly averaged LSD intensity profile was modelled to measure $v \sin i$. For the 36 stars for which more than one observation is available, the standard deviations of the $v \sin i$ values reported in Paper I are less than 10 per cent of the mean $v \sin i$ value, with the exception of HD 167262. A visual inspection of the LSD profiles for this star does not show significant variation in total line broadening – the lower values of $v \sin i$ reported in Paper I were accompanied with larger values of macroturbulence velocities. Column 5 of Table 2 lists, for each star, the $v \sin i$ averaged over all observations that we use in our modelling in Section 3.

3 BAYESIAN MODELLING

We compared the LSD profiles of each star to a grid of synthetic Stokes V profiles using the method of Petit & Wade (2012). In this approach, we assume a simple centred dipolar field model $M_{B_{\rm pole}}$, parametrized by the dipole field strength $B_{\rm pole}$, the rotation axis inclination i with respect to the line of sight, the positive magnetic axis obliquity β, and a set of rotational phases $\Phi = [\varphi_1 \dots \varphi_N]$ associated with a set of Stokes V observations of a single star.

Given that the rotation periods of the survey stars are effectively unknown, we treat the rotational phases as nuisance parameters to obtain the goodness of fit of a given rotation-independent $\mathcal{B} = [B_{\rm pole}, i, \beta]$ magnetic configuration in a Bayesian statistical framework

$$p(\mathcal{B}|\mathcal{D}, M_{B_{\rm pole}}) = \int \frac{p(\mathcal{B}, \Phi|M_{B_{\rm pole}}) p(\mathcal{D}|\mathcal{B}, \Phi, M_{B_{\rm pole}})}{p(\mathcal{D}|M_{B_{\rm pole}})} {\rm d}\Phi. \quad (1)$$

The Bayesian prior for the inclination is described by a random orientation $[p(i|M_1) = \sin(i)\,{\rm d}i]$. Given that the inclination angle cannot be strictly 0° if rotational broadening is present ($v \sin i > 0$), we restrict the range of inclination angle values explored to angles larger than $i > \sin^{-1}(v_{\rm eq} \sin i / v_{\rm eq,max})$. We can estimate $v_{\rm eq,max}$ by the breakup velocity of the stars ($V_{\rm crit} = \sqrt{GM/1.5R_{\rm pole}}$). We adopt a conservatively overestimated value of 700 km s^{-1} for the whole sample. A overestimation of $v_{\rm eq,max}$ leads to the inclusion of smaller inclinations in the parameter space. This in turn gives less weight to the inclination angles of around 90°, which are more likely to produce a low amplitude or no Stokes V signal. We may therefore slightly overestimate the magnetic field upper limits, although not by much, as the prior probabilities for low-inclination configurations are low.

The dipole field strength $B_{\rm p}$ is a parameter that can vary over several decades (from a few dozen gauss to a few kilogauss). We therefore used a Jeffreys prior, which sets an equal probability per decade and therefore represents a lack of information about the scale of the parameter. To avoid a singularity at $B_{\rm pole} = 0$ G, we used the modified form of Gregory (2005). The obliquity and the rotational phases have constant priors, appropriate for positional parameters.

The synthetic flux profiles are obtained by numerically integrating the emergent intensities over the projected stellar disc of a given magnetic geometric configuration. We use a limb darkening law of the form $I(\mu)/I(\mu = 1) = 1 - \epsilon + \mu\epsilon$, where μ is the cosine of the angle between the ray direction and the normal to the stellar surface. As we are using line profiles resulting from the LSD method (with spectral lines covering a broad range of visible wavelengths), we use the fiducial, grey value of $\epsilon = 0.6$ for the whole sample.

The emergent intensities are calculated using the weak-field approximation described by Landi degl'Innocenti & Landolfi (2004). For this study, we use Voigt-shaped line profiles with a damping constant $a = 10^{-2}$ and a thermal speed $v_{\rm th} = 7$ km s^{-1}, appropriate for the stellar temperatures under consideration as the LSD profiles are mostly composed of metallic spectral lines.

Table 2. Results from our Bayesian analysis. The columns report (1) a reference number with binarity status, (2) the name of the star with (3) its spectral type reproduced from Paper I, (4) the number of nightly averaged observations, (5) the rotational broadening adopted in our models, the odds ratio $\log(M_{B_p=0}/M_{B_p})$ obtained from (6) the Stokes *V* and (7) the null profiles, (8) the upper limit to the 68.3 per cent credible region obtained from Stokes *V*, (9) same as the previous column for the 95.4 per cent credible region, (10, 11) same as the previous two columns for the null profiles, and the mode of the probability density function marginalized for B_p obtained from (12) Stokes *V* and (13) the null profiles. The bold entries highlight odd ratios $\log(M_{B_p=0}/M_{B_p}) < -0.5$ for easy reference.

ID	Name	Spectral type	N_{obs}	$v \sin i$ (km s^{-1})	Odds *V*	Odds N	68 *V* (G)	95 *V* (G)	68 N (G)	95 N (G)	Mode *V* (G)	Mode N (G)
(1)	(2)	(3)	(4)	(5)	(6)	(7)	(8)	(9)	(10)	(11)	(12)	(13)
1 SB2	HD 1337 A	O9.5 II(n)	1	118	0.02	0.41	212	549	63	225	132	0
2	HD 1337 B		1	23	0.28	0.32	275	1187	232	931	0	0
3	HD 13745	O9.7 II(n)	3	170	0.2	0.46	177	491	105	314	0	0
4	HD 14633	ON8.5 V	1	120	0.5	0.19	58	209	118	372	0	0
5 SB3	HD 17505 Aa1	O6.5 IIIn((f))	1	8	0.27	0.28	423	1976	358	1727	0	0
6	HD 17505 Ab		1	14	0.3	0.22	435	1921	585	2922	0	0
7	HD 17505 Aa2		1	1	0.16	0.26	614	2628	413	2075	0	0
8	HD 24431	O9 III	1	60	0.29	0.18	48	162	70	218	0	0
9	HD 24534	O9.5npe	1	200	**−0.73**	0.42	632	1414	123	443	387	0
10	HD 24912	O7.5 III(n)((f))	13	201	0.64	**−1.27**	13	37	50	125	0	27
11	HD 30614	O9 Ia	5	96	0.64	0.54	16	47	19	56	0	0
12	HD 34078	O9.5 V	4	16	0.67	0.9	29	69	16	49	0	0
13	HD 34656	O7.5 II(f)	1	70	0.37	0.39	52	185	41	148	0	0
14	HD 35619	O7.5 V	1	45	0.18	0.31	108	341	72	248	0	0
15 SB2	HD 35921	O9.5 II	1	205	0.42	0.42	103	370	125	448	0	0
16[a]	HD 36486	O9.5 IINwk	2	121	**−2.46**	0.64	94	242	21	70	56	0
17	HD 36512	O9.7 V	1	18	0.48	0.17	33	122	86	255	0	0
18	HD 36861	O8 III((f))	8	61	0.61	0.65	14	35	12	35	0	0
19	HD 36879	O7 V(n)((f))	2	185	0.52	**−0.98**	55	180	259	556	0	154
20 SB2	HD 37041	O9.5 Ivp	3	123	−0.03	0.58	84	193	31	93	0	0
21 SB2	HD 37043	O9 III var	1	78	0.02	0.35	80	220	30	104	0	0
22 SB2	HD 37366	O9.5 IV	1	2	0.25	0.32	40	207	29	167	0	0
23 SB2	HD 37468	O9.7 III	1	118	**−1.62**	0.22	182	406	56	180	112	0
24	HD 38666	O9.5 V	1	114	0.37	−0.35	38	135	100	273	0	0
25	HD 42088	O6 V((f)z	1	37	0.32	0.38	113	382	85	303	0	0
26	HD 46056	O8 Vn	1	344	0.31	0.37	371	1279	294	997	0	0
27 SB2	HD 46106	O9.7 II-III	1	86	0.44	0.37	88	317	124	429	0	0
28 SB2	HD 46149	O8.5 V	3	40	0.38	0.55	70	309	38	114	0	0
29	HD 46150	O5 V((f))z	3	86	−0.80	−0.05	160	298	108	276	0	0
30	HD 46202	O9.5 V	2	20	0.43	0.48	31	94	28	92	0	0
31	HD 46223	O4 V((f))	2	67	0.23	0.41	126	344	77	248	0	0
32	HD 46485	O7 Vn	3	312	0.51	0.38	127	379	192	530	0	0
33	HD 46966	O8.5 IV	1	50	0.43	0.39	39	139	39	137	0	0
34	HD 47432	O9.7 Ib	1	90	0.42	0.28	30	108	47	161	0	0
35[a]	HD 47839	O7 V((f)) var	8	50	0.68	0.49	15	43	27	68	0	0
36 SB2	HD 48099 A	O6.5 V(n)((f))	2	91	0.27	0.54	82	226	41	141	0	0
37	HD 48099 B		2	51	0.63	0.58	52	184	58	190	0	0
38 SB2	HD 54662 A	O7 V((f))z var?	1	31	0.34	0.32	53	181	57	191	0	0
39	HD 54662 B		1	148	0.37	0.24	87	304	137	423	0	0
40	HD 55879	O9.7 III	1	36	0.35	0.36	16	60	17	60	0	0
41	HD 66788	O8 V	2	24	0.3	0.37	200	556	147	460	0	0
42	HD 66811	O4 If	2	185	0.46	**−0.61**	32	101	140	322	0	0
43	HD 69106	O9.7 In	1	312	0.41	0.38	100	362	115	415	0	0
44	HD 93028	O9 IV	1	20	0.28	0.34	129	447	122	465	0	0
45[a]	HD 93250	O4 IIIfc:	1	50	0.15	0.15	496	1755	435	1442	0	0
46	HD 149038	O9.7 Iab	1	66	0.3	0.3	28	94	28	96	0	0
47	HD 149757	O9.5 Ivnn	45	352	0.77	0.6	47	129	76	180	0	0
48	HD 151804	O8 Iaf	1	78	0.36	0.18	57	201	81	255	0	0
49	HD 152233	O6 III(f)	1	75	0.22	0.36	120	367	74	262	0	0
50	HD 152247	O9.5 II-III	1	80	0.19	0.06	245	776	328	939	0	0
51	HD 152249	OC9 Iab	1	80	0.39	0.26	36	131	58	187	0	0
52	HD 152408	O8 Iafpe	1	78	0.29	0.26	139	469	159	513	0	0
53 SB2	HD 153426	O9 II-III	2	94	0.45	−0.03	62	189	181	403	0	0
54	HD 153919	O6 Iaf	1	135	0.07	0.35	157	449	77	265	0	0
55	HD 154368	O9.5 Iab	1	73	0.4	0.34	28	102	34	118	0	0
56	HD 154643	O9.5 III	1	106	0.39	0.41	41	148	38	135	0	0
57	HD 155806	O7.5 V	4	70	0.46	0.4	35	92	36	99	0	0
58 SB2	HD 155889	O9.5 IV	1	12	0.1	0.36	198	862	98	391	0	0
59	HD 156154	O7.5 Ibf	1	78	0.41	0.4	62	221	63	224	0	0

Table 2 – *continued*

ID	Name	Spectral type	N_{obs}	$v \sin i$ (km s^{-1})	Odds V	Odds N	68 V (G)	95 V (G)	68 N (G)	95 N (G)	Mode V (G)	Mode N (G)
(1)	(2)	(3)	(4)	(5)	(6)	(7)	(8)	(9)	(10)	(11)	(12)	(13)
60	HD 162978	O8 II(f)	2	76	**−1.90**	0.42	161	289	26	81	91	0
61	HD 164492	O7.5 Vz	1	32	**−0.62**	0.34	442	880	84	306	274	0
62 SB2	HD 164794 A	O3.5 V((f*))	5	87	0.49	0.1	150	417	373	860	0	0
63	HD 164794 B	O5-5.5 V((f))	5	57	0.53	0.28	85	247	157	414	0	0
64 SB2	HD 165052 A	O5.5Vz	1	73	0.34	0.36	110	392	98	350	0	0
65	HD 165052 B	O8V	1	80	0.4	0.24	97	346	185	579	0	0
66	HD 167263	O9.5 II-IIIn	1	57	−0.19	0.3	251	589	70	253	153	0
67	HD 167264	O9.7 Iab	9	51	0.57	0.67	27	80	19	55	0	0
68[a]	HD 167771	O7 III(f)	1	50	0.21	0.25	64	198	56	190	0	0
69	HD 186980	O7.5 III((f))	1	67	0.37	0.4	37	133	37	131	0	0
70	HD 188001	O7.5 Iabf	1	89	0.18	0.27	165	504	132	419	0	0
71	HD 188209	O9.5 Iab	7	69	0.57	0.57	10	30	10	30	0	0
72	HD 189957	O9.7 III	1	84	−0.01	0.25	142	429	99	337	0	0
73[a]	HD 190918	WN5o+O9 I	2	107	0.28	0.39	118	310	97	306	0	0
74 SB2	HD 191201 A	O9.5 III	1	25	0.25	0.24	176	766	166	738	0	0
75	HD 191201 B	B0 IV	1	2	0.24	0.23	162	765	173	816	0	0
76	HD 192281	O4.5 Vn(f)	2	270	0.06	0.32	318	788	184	551	0	0
77	HD 192639	O7.5 Iabf	1	96	0.43	0.12	66	234	131	396	0	0
78 SB2	HD 193322 Aa	O9 IV(n)	1	345	0.24	0.15	411	1315	439	1425	0	0
79	HD 193322 Ab1		1	39	0.19	0.31	67	225	49	174	0	0
80 SB2	HD 193443 A	O9 III	1	79	0.35	0.34	72	246	74	255	0	0
81	HD 193443 B		1	74	0.34	0.4	215	706	168	593	0	0
82[a]	HD 199579	O6.5 V((f))z	1	35	**−1.21**	0.06	154	416	95	344	0	0
83	HD 201345	ON9.5 IV	1	90	0.37	0.35	117	406	130	438	0	0
84	HD 203064	O7.5 IIIn((f))	4	277	0.55	0.83	81	229	49	163	0	0
85 SB2	HD 204827	O9.7 III	1	71	−0.11	0.37	233	641	88	312	0	0
86	HD 206183	O9.5 IV-V	1	9	0.38	0.43	53	213	38	144	0	0
87[a]	HD 206267	O6.5 V((f))	1	40	0.23	0.22	132	491	127	460	0	0
88	HD 207198	O9 II	10	69	0.6	0.47	18	48	20	54	0	0
89	HD 207538	O9.7 IV	1	35	0.4	0.29	26	93	38	122	0	0
90 SB2	HD 209481 A	O9 IV(n) var	11	135	−0.36	0.75	102	234	33	95	58	0
91	HD 209481 B		11	85	0.3	0.71	217	446	77	217	0	0
92	HD 209975	O9 Ib	9	70	**−0.67**	0.49	35	77	14	38	21	0
93	HD 210809	O9 Iab	1	100	0.42	**−1.10**	34	124	184	419	0	117
94	HD 210839	O6.5 I(n)fp	26	220	0.15	**−3.44**	88	141	144	220	62	116
95	HD 214680	O9 V	17	26	−0.07	0.53	13	22	8	16	9	0
96	HD 218195	O8.5 III	1	61	0.41	0.27	46	163	76	250	0	0
97	HD 218915	O9.5 Iab	1	63	0.01	0.42	91	267	34	122	0	0
98	HD 227757	O9.5 V	2	18	0.39	0.38	238	701	323	1157	0	0
99	HD 258691	O9.5 IV	1	23	0.04	0.35	125	362	62	216	0	0
100	HD 328856	O9.7 II	1	98	0.39	0.07	87	308	209	595	0	0
101	BD −13 4930	O9.7 V	1	13	0.42	0.39	61	216	76	280	0	0
102	BD +60 499	O9.5 V	1	23	0.29	0.04	207	652	249	724	0	152

[a] Stars identified as binaries in Paper I, but for which an SB2 treatment was unnecessary (SB1, large luminosity ratio, etc.) or unfeasible (see notes in Appendix A).

We adjust the line depth and the isotropic Gaussian macroturbulence[1] velocity v_{mac} to fit the mean of the Stokes I LSD profiles of a given star.

We performed this analysis on the circular polarization LSD Stokes V profiles as well as the null polarization LSD profiles.

3.1 Spectroscopic binaries

We consider that the presence of a non-magnetic spectroscopic binary companion may have two effects (other than the radial velocity shift) on the LSD profiles and their analysis. First, a companion contributes continuum flux to the observed spectrum, reducing the amplitude of any Stokes V profile contributed by the primary star in the normalized circular polarization spectrum. Simultaneously, the depths of spectral lines of the star in the Stokes I spectrum are also reduced by the same factor. As a consequence, the ratio of V to I is preserved, and the net result is only to increase the inferred uncertainty of the magnetic diagnosis. In other words, the continuum flux of a companion increases the upper limit on an undetected field, but does not introduce any systematic error.

The second effect results from the presence of the spectral lines of the companion. In this case, the companion's lines may blend with those of the studied star, making the determination of the relevant velocity range for the diagnosis of Stokes V profiles ambiguous. In addition, spectral line blending contributes to the equivalent width

[1] Of the form $e^{-v^2/v_{mac}^2}/(\sqrt{\pi}v_{mac})$.

of Stokes I, but has no influence on the Stokes V profile, assuming the companion is not magnetic. Hence, uncorrected line blending of a companion may systematically affect the magnetic diagnosis. In cases where we might have failed to recognize an SB2 system and treated it as a single star, we would underestimate the maximum field strength allowed by the data for the primary by at most a factor of 2, which corresponds to the extreme case of two O-type stars with identical spectral type and luminosity.

Our sample contains 20 SB2 systems, for which we correct for the line blending effect by modelling the components' contributions to the Stokes I profile, as described in Paper I. These stars are identified in Table 2 with an 'SB2' label in column 1.

As our modelling requires a single set of line parameters for all observations, we find the best fit to the ensemble of observations that can be obtained by only adjusting the radial velocities. The fits are presented in Appendix A.

We perform our analysis as mentioned earlier by making the assumption that the secondary star does not have a magnetic field. This is reasonable as no Stokes V signal has been definitively detected in any stars in the sample adopted for analysis in this study. Therefore, to be more precise, this analysis does not take into account the possibility that the polarization from both stars cancels out – which would be relevant only for observations at an orbital phase when the spectral lines overlap significantly.

For 10 stars within the binary sample, the literature indicates that the secondary is also an O-type star. For these stars, we perform our calculation again, considering that the primary is not magnetic and the secondary might be magnetic. This makes the assumption that the mask was suitable for both sets of spectral lines – another reason to only do these calculations for O-type secondaries. In one case, HD 17505, the spectral lines from three O-stars are present: both companions were included.

3.2 Odds ratios

To assess the presence of a dipole-like signal in our observations, we compute the odds ratio of the null model ($M_{B_{\rm pole}=0}$; no magnetic field implying Stokes $V = 0$) with the dipole model ($M_{B_{\rm pole}}$)

$$\frac{M_{B_{\rm pole}=0}}{M_{B_{\rm pole}}} = \frac{p(M_{B_{\rm pole}=0})}{p(M_{B_{\rm pole}})} \frac{p(\mathcal{D}|B_{\rm pole}=0)}{p(\mathcal{D}|M_{B_{\rm pole}})}. \quad (2)$$

The resultant metric, $\log(M_{B_{\rm pole}=0}/M_{B_{\rm pole}})$, is displayed in Table 2 for Stokes V (column 6) and for the null N profiles (column 7).

In general, the odds ratios are in favour of the non-magnetic model by approximately half an order of magnitude. Note that both the magnetic and the non-magnetic model can reproduce a signal consisting of only pure noise equally well, as the case $B_{\rm pole} = 0$ G is a valid parameter of the magnetic model. Therefore, in the case of pure noise the difference between the two models is expected to be dominated by the ratio of priors that penalizes the magnetic model for its added complexity. Therefore, in this nested model we consider any odds ratios not strongly in favour of the magnetic model to indicate the absence of significant magnetic signal in the observations. According to Jeffreys (1998), the evidence in favour of a given model is considered moderate when $>10^{1.0}$ (10:1), strong when $>10^{1.5}$ (30:1), and very strong when $>10^{2.0}$ (100:1).

3.3 Probability density function

As discussed by Petit & Wade (2012), no meaningful constraint can be placed on the dipole geometry (i and β) when no circular polarization signal is present. We therefore treat the dipole geometry parameters as nuisance parameters to extract the probability density distribution for the dipolar field strength

$$p(B_{\rm pole}|\mathcal{D}, M_{B_{\rm pole}}) = \int p(\mathcal{B}|\mathcal{D}, M_{B_{\rm pole}})\, {\rm d}i\, {\rm d}\beta. \quad (3)$$

Except for stars with strong evidence in favour of the magnetic model, all the probability distributions generally peak at 0 G and have an extended tail at large field values, caused by the few dipole orientations that never result in a circular polarization signal. From this probability density, we extract the credible regions around the maximum probability value enclosing a given percentage of the integrated probability. With a Gaussian-shaped probability density, enclosed probabilities of 68.3, 95.4, and 99.7 per cent would be analogous to the 1σ, 2σ, and 3σ contours in frequentist statistics. However, our probability distributions generally deviate strongly from a Gaussian (see discussion by Petit & Wade (2012)) and these credible regions are generally not linear (i.e. the upper limit of the 99.7 per cent credible region for $B_{\rm pole}$ will generally reach farther from the peak value than three times that of the 68.3 per cent credible region). In Table 2 (columns 8–11), we compile the credible region upper limits for the 68.3 and 95.4 per cent credible regions, the latter being associated with the field strength that would generally have been detectable in the large majority of field configurations (as demonstrated by Petit & Wade (2012)).

4 STATISTICAL RESULTS

Fig. 1 (left) shows a comparison of the odds ratios $\log(M_{B_{\rm pole}=0}/M_{B_{\rm pole}})$ for the null profiles (on the y-axis) and for the Stokes V profiles (on the x-axis). The region below the horizontal line represents stars for which the magnetic model is preferred for the null profiles. Therefore, any stars located in the shaded blue region (more than 10:1 in favour of the magnetic model) are considered to possibly have instrumental spurious signal or stellar variability of non-magnetic origin.

The region to the left of the vertical line represents stars for which the magnetic model is preferred for the Stokes V profiles. Stars with Stokes V profiles yielding an odds ratio at least 10:1 in favour of the magnetic model ($\log(M_{B_{\rm pole}=0}/M_{B_{\rm pole}}) < -1$) and no evidence of significant null signal (red shaded region) are therefore considered to be magnetic candidates. These candidates are in agreement with those reported in Paper I (their table 4 and fig. 4), with the addition of the primary component of HD 37468 (Fig. 2).

In addition to the candidate magnetic stars, Paper I identifies a list of six probable spurious detections in the Stokes V profiles. These stars do not appear as such with our method – the excess Stokes V signal does not match the expected shape for a dipolar magnetic field yielding an odds ratio inferior to the 10:1 threshold ($\log(M_{B_{\rm pole}=0}/M_{B_{\rm pole}} > -1)$). We hence confirm that these are indeed spurious detections.

Paper I computed two incidence rates of magnetic stars: 5.6 ± 2.3 per cent considering only detected magnetic stars and 8.3 ± 2.8 per cent considering the magnetic candidates, yielding a mean incidence of 7 ± 3 per cent. The addition of one magnetic candidate gives 5.6 ± 2.3 and 9.3 ± 2.9 per cent, respectively, therefore not modifying the reported 7 ± 3 per cent incidence within the error bar.

The right-hand panel of Fig. 1 compares the upper limits of the credible region corresponding to 68.3 per cent of the probability, again for the null (y-axis) and the Stokes V (x-axis) profiles. The individual stars for which the odds ratio was strongly in favour of

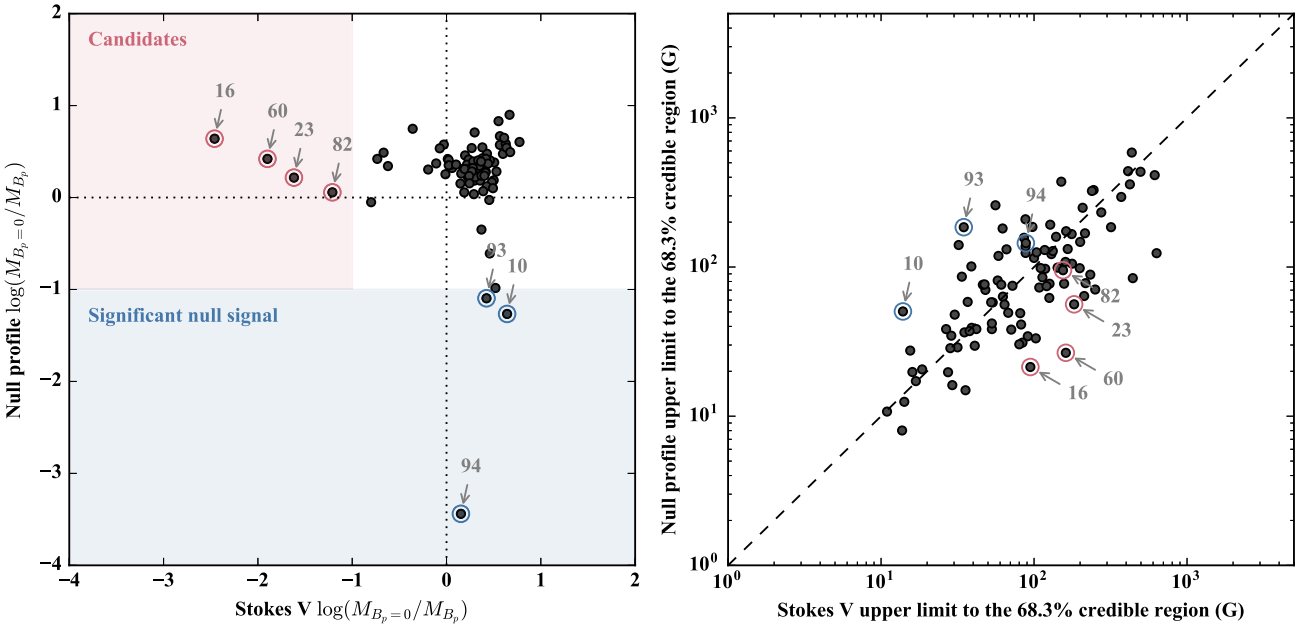

Figure 1. *Left*: Comparison of the odds ratios $\log(M_{B_{\rm pole}=0}/M_{B_{\rm pole}})$ for the null profiles and the Stokes *V* profiles. The region below the horizontal line contains stars for which the magnetic model is preferred for the null profiles. The region to the left of the vertical line contains stars for which the magnetic model is preferred for the Stokes *V* profiles. The blue shaded region indicates odds ratios indicative of significant null signal. The red shaded region indicates the location of magnetic candidates. Specific stars discussed in the text are labelled with their identification number as assigned in Table 2. *Right:* Upper limits of the credible region corresponding to 68.3 per cent of the probability, for the null profiles and for the Stokes *V* profiles. The dashed line shows the one-to-one correspondence.

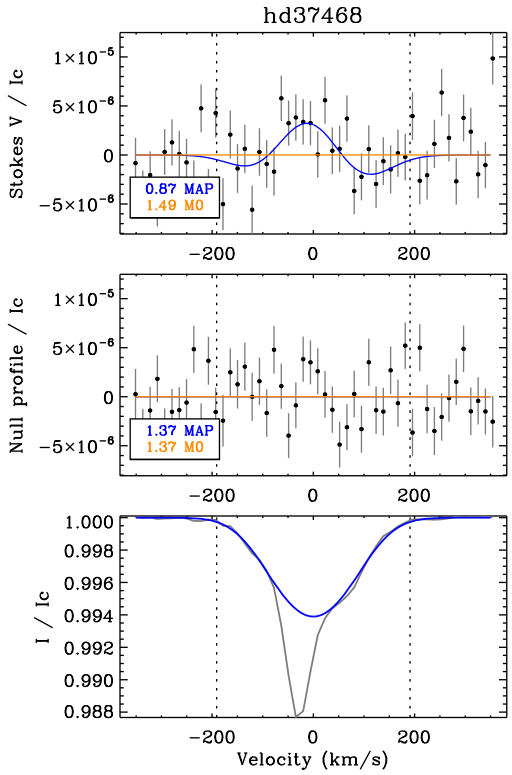

Figure 2. LSD profile of the magnetic candidate HD 37468 (#23). The bottom, middle, and top panels show the intensity, null, and Stokes *V* profiles, respectively. The non-magnetic model (MO) and the model with the maximum a posteriori probability (MAP) are shown in orange and blue, respectively. The corresponding reduced χ^2 are indicated in the legends.

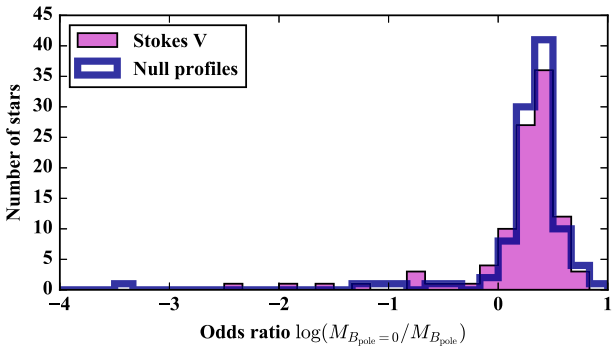

Figure 3. Distributions of odds ratios derived from the Stokes *V* profiles and from the null profiles, most likely drawn from the same parent distribution.

the magnetic model, either for the null profile or for the Stokes *V* profiles, are circled in blue and red, respectively. In general, the upper limits for our sample show a correspondence between the null profiles and Stokes V profiles with a standard deviation of ∼0.3 dex.

We thus conclude that apart from the three magnetic candidate stars identified by Paper I and the additional magnetic candidate identified in this study, there is no strong evidence for a magnetic signal in any other individual star in our sample.

We now analyse our sample as a population, to determine which types of magnetic field strength distributions would be compatible with our measurements.

4.1 Population analysis

In Fig. 3, we compare the distribution of odds ratios derived from the Stokes *V* profiles and the null profiles (filled red histogram

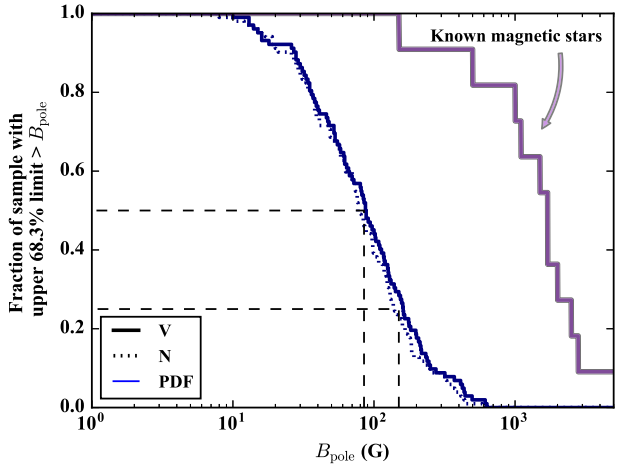

Figure 4. Cumulative histograms of the fraction of the sample with an upper limit to the 68.3 per cent credible region *larger* than a certain dipole strength value $B_{\rm pole}$, for the Stokes *V* profiles (solid blue) and the null profiles (dotted blue). The black dashed lines illustrate that (i) 25 per cent of the stars in our sample have upper limits larger than the lowest, detected magnetic field in an O-type star (∼140 G; Blazère et al. 2015), and (ii) half of the stars in our sample have 68.3 per cent upper limits better than 85 G. The cumulative histogram of the currently known magnetic O-type stars (in pink) is illustrated as the fraction of magnetic stars with a dipolar field strength larger than $B_{\rm pole}$.

and empty blue histogram, respectively).[2] A Kolmogorov–Smirnov (KS) test results in a 69 per cent probability that these two distribution are likely drawn from the same parent distribution. This implies that the odds ratios derived from the Stokes *V* profiles are consistent with the instrumental noise as represented by the null profiles.

Fig. 4 shows cumulative histograms of the fraction of the sample with an upper limit to the 68.3 per cent credible region that is larger than a certain dipole strength value. The distribution for the Stokes *V* profiles (solid dark blue) agrees with the null profile distribution (dashed dark blue) – a KS test results in a ∼90 per cent probability that these two samples were drawn from the same parent distribution.

We compare these to the distribution of dipolar field strengths of the 11 known magnetic O-type stars, illustrated in Fig. 4 as the fraction of magnetic stars with a dipolar field strength larger than a certain value.[3] We use the magnetic strength values reported in the compilation of Petit et al. (2013), with the addition of the magnetic O-type star HD 54879 subsequently detected by Castro et al. (2015). A KS test results in a 10^{-5} probability that the distribution of the 68.3 per cent upper limits and the distribution of the known magnetic field strengths are drawn from the same distribution. Even when considering the upper limits of the 99.7 per cent credible region, a KS test also indicates that they are not compatible (10^{-2} probability that they are drawn from the same distribution).

Thus, at first glance, we can conclude that if all the stars in our sample host a magnetic field just below their detection limit, the distribution in strength of these undetected fields would be different from the distribution in strength of the known magnetic O-type stars. This could suggest a bimodal distribution of magnetic fields, grouped in separate – very weak or very strong – regimes. However, this simple comparison might not be viewed as fair, given the expected evolution of surface fields with age, which we will address in Section 5.

However, first we set out to address the following question: could *all* of the O-type stars in the sample have a magnetic field slightly weaker than the current, average observation limits? As all the stars in our sample have various detection limits due to factors such as brightness, signal-to-noise ratio of the observations, line broadening, number of spectral lines available for LSD multiline technique, etc., the best way to explore this question is through a Monte Carlo simulation.

We perform a Monte Carlo simulation by calculating sets of synthetic Stokes *V* signatures corresponding to a dipolar magnetic field with a polar strength of 100 G. This rounded field value corresponds roughly to the upper limit of the 63.8 per cent credible region achieved for 50 per cent of the sample. It also corresponds to the order of magnitude in field strength at which the magnetic desert is observed.

For each star, the geometry of the dipolar field (i and β) and the observational rotational phases (Φ) are randomly selected. All these parameters are drawn from a uniform distribution, apart from the inclination of the rotational axis that is drawn from a sin (i) distribution (as discussed in Section 3). The characteristics of the intensity profiles are the same as those used for the real sample. The corresponding synthetic magnetic signal is injected directly into the real null profile signal, which is a direct measure of the noise of each individual LSD profile. The Bayesian probability distributions and odds ratios were recalculated using these new profiles. We performed 30 realizations of this Monte Carlo simulation over our sample.

Fig. 5 (left) shows the fraction of the sample with an odds ratio more than 10:1 (light pink), and 100:1 (dark blue) in favour of the magnetic model for each Monte Carlo realization. The unambiguously detected fraction in the simulated sample is ∼15 per cent. In other words, 15 per cent of this synthetic sample (i.e. ∼15 stars) of uniformly magnetized stars would have been detected in the MiMeS survey, while 85 per cent would have remained undetected. However, the right-hand panel of Fig. 5 shows a histogram (in light pink) of KS test values between the observed distribution of odds ratios obtained from the null profile and the distribution of odds ratios for each Monte Carlo realization. In comparison to the good agreement between the observed distribution calculated from the Stokes *V* and null profiles, as indicated by the high value obtained for the KS test (dark blue dashed line in Fig. 5), the distribution of odds ratios resulting from the Monte Carlo simulations is significantly different from the observed distribution from the null profiles. This is also the case when comparing the Monte Carlo distributions to the observed odds ratio distributions obtained from the Stokes *V* profiles instead of the ones from the null profiles. Fig. 6 (left) also compares the distribution of 68.3 per cent credible region upper limits obtained for each Monte Carlo simulation (grey curves) with the observed distributions from the Stokes *V* and null profiles. Once again, a KS test between these simulated distributions and the observed Stokes *V* and null distributions shows that they are significantly different – the right-hand panel of Fig. 6 shows the histogram of KS values (in light pink) once again compared to the KS value between the observed distribution calculated from the Stokes *V* and null profiles (in dark blue).

We therefore conclude that even though the direct detection rate would be rather low – only slightly higher than the measured

[2]The inclusion or exclusion of the candidate magnetic stars or of the stars with significant null signal does not change the final conclusions. In the following discussion, we consider the full sample.

[3]The magnetic star distribution does not reach zero in our figure, as NGC 1624-2 has a field of 20 kG, outside the range of our figure.

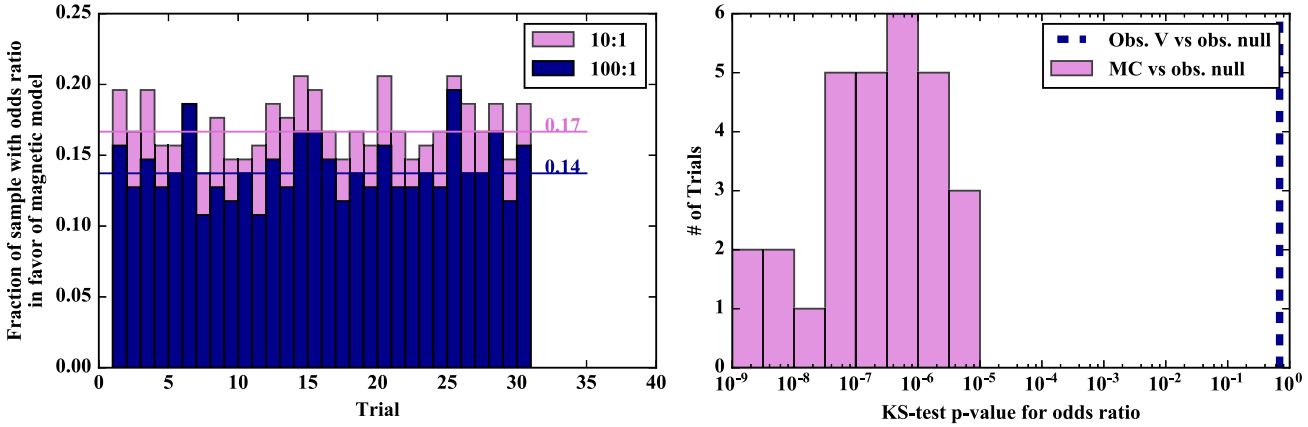

Figure 5. Results from 30 Monte Carlo calculations in which the signal from a 100 G dipolar field with a random orientation was injected into the N profile in every star. *Left*: Number of stars for which the odds ratio is greater than 10:1 and 100:1 in favour of the magnetic model, in light pink and dark blue, respectively. The mean fraction for each threshold is indicated by the horizontal line of the appropriate colour. *Right:* Histogram of KS test values calculated between the observed distribution of odds ratios for the original null profile and each Monte Carlo distribution (in light pink). This is compared with the good agreement between the observed distribution of odds ratio for Stokes *V* and for the null profile (dark blue dashed line).

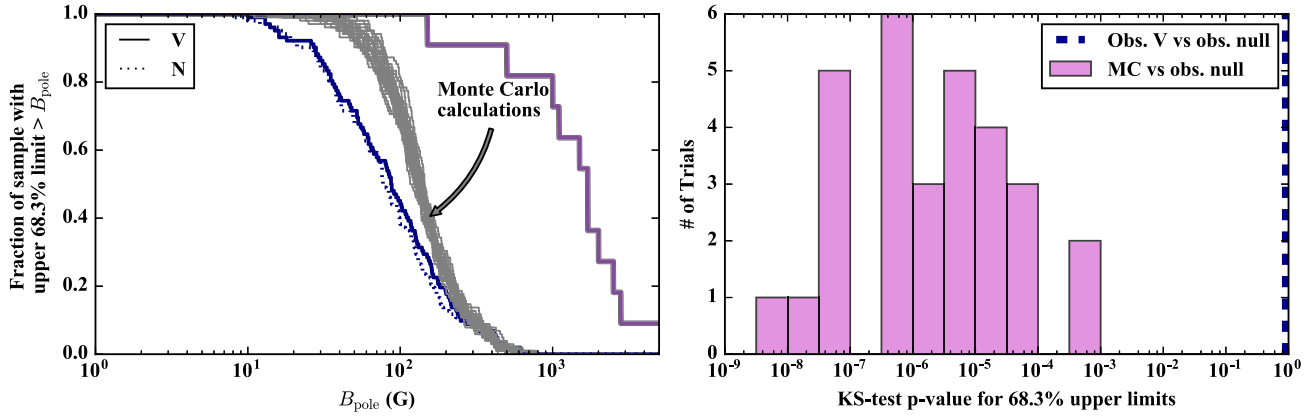

Figure 6. Results from 30 Monte Carlo calculations in which the signal from a 100 G dipolar field with random orientation was injected into the null profile for every star. *Left*: Same as Fig. 4, with the addition of the distribution of 68.3 per cent upper limits for each Monte Carlo calculation (grey histograms). *Right*: Same as the right-hand panel of Fig. 5, but for the distribution of 68.3 per cent upper limits.

bulk incidence of magnetism in massive stars – the presence of a 100 G dipolar field in every star in our sample would have resulted in a distribution of odds ratio from the Stokes *V* profiles that is statistically different from those obtained from the null profiles. In other words, if all the stars had a 100 G field, we would have noticed. The same is also true for the distributions of credible region upper limits. To test whether this result is simply driven by a small number of very high quality observations, we also remove from the sample the simulated observations that yield an odds ratio greater than 10:1 in favour of the magnetic model and recalculate the KS tests. The results lead to the same conclusion.

4.2 Completeness of the MiMeS O-star survey

Our Monte Carlo calculations also provide a way to quantify the completeness of the MiMeS survey of O-type stars to the detection of a star with a magnetic field of a certain strength. From the case presented in the previous subsection, injecting a simulated Stokes *V* signature in every star in our sample only yields an unambiguous detection (from the odds ratios) for 15 per cent of the sample. For a 500 G field, this fraction goes up to 70 per cent. Let us consider a sample of O-type stars with the same characteristics as the MiMeS sample containing only one magnetic star, with a dipolar strength of 100 G/500 G. This 15/70 per cent can be thought of as the probability of detecting that magnetic star among the sample. In fact, these fractions obtained from the Monte Carlo calculations follow closely the cumulative distribution constructed from the upper limits to the 95.4 per cent credible regions for $B_{\rm pole}$.

In Fig. 7, we present this cumulative distribution, as a proxy for the completeness of the MiMeS survey of O-type stars with respect to magnetic field strength. The cumulative distribution of field strengths for the known magnetic O-type stars is also shown as a reference. The survey is nearly complete for dipolar magnetic field at the kilogauss level (the top dashed line indicate 90 per cent completeness), and 50 per cent complete at the 250 G level (lower dashed line).

5 DISCUSSION

In this section, we discuss two applications of our sample of upper limits: (i) evaluating the role of observational biases in the observed deficit of old magnetic stars and (ii) searching for evidence of a magnetic desert in O-type stars.

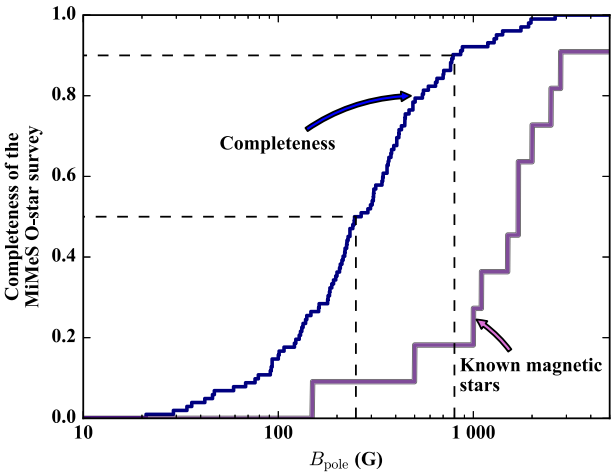

Figure 7. Completeness of the MiMeS survey of O-type stars derived from the cumulative distribution of the upper limits to the 95.4 per cent credible regions for $B_{\rm pole}$. The cumulative distribution of field strengths for known magnetic O-type stars is shown as a reference. The dashed lines illustrates the 50 and 90 per cent completeness levels.

5.1 Observational bias in the detection of old magnetic stars

As discussed in Section 1, F2016 found evidence suggesting a deficit of old magnetic stars by comparing the ages of known magnetic OB stars with those of a magnitude-limited control sample of OB stars.

One possible explanation of this result is that the sample of known magnetic stars is somewhat observationally biased. The estimation of magnetic field detectability performed by F2016 indicated that most of the known magnetic OB stars would still be detectable on the TAMS with present-day instrumentation under the magnetic flux conservation hypothesis. We here test whether this result holds using our sample of O-type stars for which magnetic detection limits are known, by determining (i) whether stars near the TAMS have been studied to detect magnetic fields and (ii) whether these stars have been observed with a magnetic detection threshold sufficient to allow for detection of the expected surface field strength under the hypothesis of magnetic flux conservation.

5.1.1 Evolutionary status of the O-stars observed by MiMeS

In order to derive evolutionary ages in the same fashion as F2016, we select stars in our sample whose physical parameters have already been homogeneously determined by Martins et al. (2015, hereafter M2015) using CMFGEN (Hillier & Miller 1998) to model the same MiMeS spectra (Grunhut et al. 2017) that are used here.

Table 3, which contains the BONNSAI results described later, lists all the stars in the MiMeS O-type star sample in the same order as in Table 2. Empty entries indicate stars not included in the analysis of M2015 (for reasons described later).

M2015 excluded known double-lined spectroscopic binaries from their sample. Of the 20 binaries (and their 11 associated O-star companions) included in our O-type star upper limit analysis, only 4 stars remain. This subsample of 67 stars is thus biased against those systems. Furthermore, eight seemingly single stars were only included in the final MiMeS O-type star sample after the parameter modelling of M2015 was performed. While these stars were therefore also excluded from the following analysis, they are not representative of a particular class or property, and thus likely do not introduce any obvious bias.

Fig. 8 shows that the upper limit distributions of the M2015 sample (thick histogram) are similar to that of the full MiMeS O-star sample (thin histogram). The grey histograms show the upper limit distributions for the Monte Carlo trials with 100 G injected in all stars, restricted to the stars in the M2015 sample. Compared to the Monte Carlo trials for the full O-type star sample in Fig. 6, this subset has similar upper limits.

We use the Bayesian code BONNSAI[4] (Schneider et al. 2014, 2017) to infer the fractional main-sequence ages τ and other stellar parameters of the M2015 sample. To this end, we match the observed surface gravity $\log g$, effective temperatures $T_{\rm eff}$, and projected rotational velocities $v \sin i$ against the stellar models of Brott et al. (2011) of solar metallicity. For the prior distributions, we use a Salpeter-like mass function for initial masses (Salpeter 1955), a uniform distribution for stellar ages, the observed Gaussian distribution of rotational velocities of Milky Way stars of Hunter et al. (2008) for $v \sin i$, and that all rotation axes are randomly oriented in space. We also checked for differences in the inferred stellar parameters when taking correlations of $\log g$ and $T_{\rm eff}$ into account as has been done by F2016 for their stellar sample. The resulting τ distributions were unaffected. We here present stellar parameters without taking correlations into account as the exact correlations of $\log g$ and $T_{\rm eff}$ for each star are unknown in our case because of a different technique that has been used to determine the atmospheric parameters (M2015). The derived fractional main-sequence ages used in the discussion later are listed in Table 3.

Fig. 9 shows the histogram of the fractional main-sequence age (τ) constructed from the sum of each star's posterior probability density, marginalized over all other fitted parameters in the Bayesian framework. In other words, each star contributes to multiple τ bins, with a distribution following its posterior probability. The sample of MiMeS O-type stars in the M2015 sample (in green) is compared with the magnitude-limited control sample of F2016 that we modified to include only the O-type stars[5] (in blue). The two fractional MS age distributions are qualitatively very similar, both peaking at ~75 per cent of the main-sequence lifetime.

From this, we conclude that the MiMeS survey did indeed observe a significant number of O-type stars that are in the second half of their main-sequence lifetime. This therefore implies that the inferred deficit of old magnetic O-type stars is not caused by a lack of observations of more evolved stars by spectropolarimetric surveys.

5.1.2 Is the MiMeS sample good enough to test models of MS field evolution?

Now, we seek to determine whether the more evolved stars in the MiMeS O-type star sample have been observed with sufficient precision to detect magnetic fields of the typical strength expected under the magnetic flux conservation hypothesis, i.e. that the surface field strength decreases with time (t) as $B(t)/B_0 = (R_0/R(t))^2$, where B_0 and R_0 are the surface field strength and radius at an earlier time, respectively.

Our reasoning is that if we find that these expected field strengths at the TAMS would have led to unambiguous detections within the capabilities of the MiMeS survey, we can rule out that the

[4]The BONNSAI web service is available at http://www.astro.uni-bonn.de/stars/bonnsai.

[5]The resulting distribution is very similar to the distribution of OB stars presented by F2016, with a slight shift of the peak of the distribution towards older ages.

Table 3. Results from the BONNSAI analysis. Columns 1–3 are reproduced from Table 2.

ID	Name	Spectral type	Age (Myr)	$M_\star$ ($M_\odot$)	$R_\star$ ($R_\odot$)	MS fractional age
(1)	(2)	(3)	(4)	(5)	(6)	(7)
1 SB2	HD 1337 A	O9.5 II(n)				
2	HD 1337 B					
3	HD 13745	O9.7 II(n)	4.32	30	19.81	0.85
4	HD 14633	ON8.5 V	3.94	22	8.16	0.66
5 SB2	HD 17505 Aa1	O6.5 IIIn((f))				
6	HD 17505 Ab					
7	HD 17505 Aa2					
8	HD 24431	O9 III	4.22	22	8.72	0.7
9	HD 24534	O9.5npe				
10	HD 24912	O7.5 III(n)((f))	3.88	25	10.93	0.71
11	HD 30614	O9 Ia	4.42	26	17.38	0.84
12	HD 34078	O9.5 V	4.14	18	6.2	0.48
13	HD 34656	O7.5 II(f)	3.22	26	9.4	0.66
14	HD 35619	O7.5 V	3.5	22	7.29	0.55
15 SB2	HD 35921	O9.5 II				
16[a]	HD 36486	O9.5 IINwk				
17	HD 36512	O9.7 V	4.36	18	6.22	0.48
18	HD 36861	O8 III((f))	3.58	24	9.08	0.66
19	HD 36879	O7 V(n)((f))	3.06	28	9.64	0.62
20 SB2	HD 37041	O9.5 Ivp				
21 SB2	HD 37043	O9 III var				
22 SB2	HD 37366	O9.5 IV				
23 SB2	HD 37468	O9.7 III				
24	HD 38666	O9.5 V	4.08	19	6.2	0.45
25	HD 42088	O6 V((f)z	2.44	27	7.38	0.41
26	HD 46056	O8 Vn	3.9	24	8.68	0.63
27 SB2	HD 46106	O9.7 II-III	5.84	16.6	7.26	0.68
28 SB2	HD 46149	O8.5 V				
29	HD 46150	O5 V((f))z	1.52	38	8.82	0.4
30	HD 46202	O9.5 V	1.14	18	5.57	0.1
31	HD 46223	O4 V((f))	1.34	41	9.23	0.37
32	HD 46485	O7 Vn	3.34	26	9.4	0.59
33	HD 46966	O8.5 IV	3.5	22	7.29	0.55
34	HD 47432	O9.7 Ib	4	30	20.5	0.85
35[a]	HD 47839	O7 V((f)) var				
36 SB2	HD 48099 A	O6.5 V(n)((f))				
37	HD 48099 B					
38 SB2	HD 54662 A	O7 V((f))z var?				
39	HD 54662 B					
40	HD 55879	O9.7 III	5.5	20	10.28	0.78
41	HD 66788	O8 V	3.54	21	6.52	0.44
42	HD 66811	O4 If	2.12	40	12.4	0.56
43	HD 69106	O9.7 In	6.36	20	12.33	0.82
44	HD 93028	O9 IV				
45[a]	HD 93250	O4 IIIfc:	1.62	45	12.02	0.47
46	HD 149038	O9.7 Iab	5.16	24	16.45	0.86
47	HD 149757	O9.5 Ivnn	5.84	20	9.7	0.71
48	HD 151804	O8 Iaf	2.1	40	28.42	0.81
49	HD 152233	O6 III(f)				
50	HD 152247	O9.5 II-III	4.88	22	10.25	0.77
51	HD 152249	OC9 Iab	3.62	31	18.65	0.81
52	HD 152408	O8 Iafpe				
53 SB2	HD 153426	O9 II-III	3.98	21.6	8.16	0.66
54	HD 153919	O6 Iaf	1.82	50	20.76	0.68
55	HD 154368	O9.5 Iab	3.62	31	18.65	0.81
56	HD 154643	O9.5 III	5.46	20	10.28	0.78
57	HD 155806	O7.5 V	3.02	23	6.83	0.44
58 SB2	HD 155889	O9.5 IV	3.92	19.2	6.18	0.48
59	HD 156154	O7.5 Ibf	3.88	28	13.29	0.75
60	HD 162978	O8 II(f)	3.7	30	13.41	0.72
61	HD 164492	O7.5 Vz	0.62	26	6.65	0.04
62 SB2	HD 164794 A	O3.5 V((f*))				
63	HD 164794 B	O5-5.5 V((f))				

Table 3 *– continued*

ID	Name	Spectral type	Age (Myr)	$M_\star$ ($M_\odot$)	$R_\star$ ($R_\odot$)	MS fractional age
(1)	(2)	(3)	(4)	(5)	(6)	(7)
64 SB2	HD 165052 A	O5.5Vz				
65	HD 165052 B	O8V				
66	HD 167263	O9.5 II-IIIn	5.18	22	12.07	0.79
67	HD 167264	O9.7 Iab	4.34	28	21.56	0.87
68[a]	HD 167771	O7 III(f)	3.52	29	11.79	0.7
69	HD 186980	O7.5 III((f))	3.52	29	11.79	0.7
70	HD 188001	O7.5 Iabf	3.38	34	16.24	0.76
71	HD 188209	O9.5 Iab	3.92	30	19.26	0.83
72	HD 189957	O9.7 III	5.48	20	10.28	0.78
73[a]	HD 190918	WN5o+O9 I				
74 SB2	HD 191201 A	O9.5 III				
75	HD 191201 B	B0 IV				
76	HD 192281	O4.5 Vn(f)	2.4	37	11.8	0.59
77	HD 192639	O7.5 Iabf	2.96	38	17.92	0.74
78 SB2	HD 193322 Aa	O9 IV(n)				
79	HD 193322 Ab1					
80 SB2	HD 193443 A	O9 III	4.88	21.8	10.25	0.77
81	HD 193443 B					
82[a]	HD 199579	O6.5 V((f))z	1.18	35	8.02	0.13
83	HD 201345	ON9.5 IV	3.7	20	6.53	0.44
84	HD 203064	O7.5 IIIn((f))	4.04	25	10.93	0.69
85 SB2	HD 204827	O9.7 III				
86	HD 206183	O9.5 IV-V	3.52	18	5.86	0.3
87[a]	HD 206267	O6.5 V((f))				
88	HD 207198	O9 II	4.36	25	12.42	0.76
89	HD 207538	O9.7 IV	5.92	17	7.72	0.71
90 SB2	HD 209481 A	O9 IV(n) var				
91	HD 209481 B					
92	HD 209975	O9 Ib	4.46	25	15.19	0.82
93	HD 210809	O9 Iab	4.46	25	15.19	0.82
94	HD 210839	O6.5 I(n)fp	3.18	34	13.41	0.68
95	HD 214680	O9 V	3.22	21	6.45	0.36
96	HD 218195	O8.5 III	3.98	22	8.16	0.66
97	HD 218915	O9.5 Iab	4.18	28	18.12	0.83
98	HD 227757	O9.5 V	3.72	20	6.53	0.44
99	HD 258691	O9.5 IV	3.92	19	6.18	0.48
100	HD 328856	O9.7 II	5.22	23	13.16	0.82
101	BD −13 4930	O9.7 V	3.52	18	5.86	0.3
102	BD +60 499	O9.5 V	3.72	20	6.53	0.44

[a] Stars identified as binaries in Paper I, but for which an SB2 treatment was unnecessary (SB1, large luminosity ratio, etc.) or unfeasible (see notes in Appendix A).

observational lack of old magnetic O-type stars is caused by a detectability bias.

Fig. 10 (left) shows the distribution of the 68.3 per cent upper limits from the MiMeS sample of M2015, separated into two subsamples according to the peak of their fractional main-sequence age probability distribution. The 'old' sample contains the 20 stars with a peak age greater than 75 per cent of their main-sequence lifetime (thick blue histogram). The 'young' sample contains the 23 stars with a peak age less than 50 per cent of the main-sequence lifetime (thick green histogram). These age thresholds were chosen to separate the two groups as much as possible in fractional age, while still retaining a large enough sample of stars in each group.

At first glance, we can see that older O-type stars in the MiMeS sample have somewhat better magnetic upper limits than younger stars (median values of the 68.3 per cent upper limits for each sample are 64 and 96 G, respectively), presumably due to their higher luminosity and slower rotation. However, we also need to assess whether these better upper limits can counterbalance the expected decrease in surface field strength.

We do so by performing the same experiment as F2016 (their section 4.1). In this experiment, we calculate the expected field strengths that the *known* magnetic O-type stars will have at the TAMS, assuming the surface magnetic flux is conserved from the current age. We then compare this distribution with the upper limit distribution for the old O-type stars in the MiMeS sample.

This comparison comes with some caveats:

(i) The middle panel of Fig. 10 shows the distribution of field strengths for the seven known magnetic O-type stars in the sample of F2016 (rightmost thick pink histogram). F2016 applied a magnitude and luminosity class cut to their samples of magnetic and non-magnetic stars, therefore rejecting four known magnetic O-type

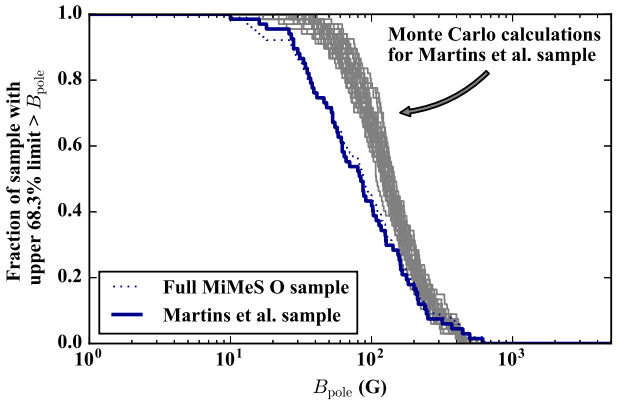

Figure 8. Cumulative histograms of the fraction of the sample with an upper limit to the 68.3 per cent credible region *larger* than a certain dipole strength value $B_{\rm pole}$, for the Stokes V profiles. The histogram for the full MiMeS O-star sample (thin dotted blue) is compared to the sample of stars in the M2015 (thick solid blue). The Monte Carlo calculations with a dipolar field of 100 G, restricted to the stars in the M2015 sample, are shown in grey.

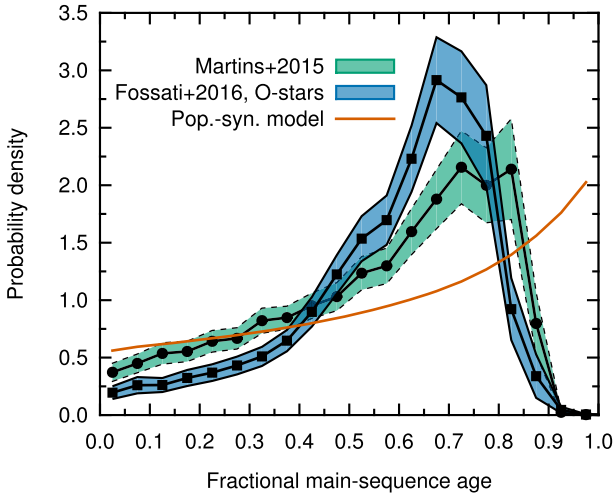

Figure 9. Fractional MS τ distributions of (i) the subsample of the MiMeS O-type star sample analysed by M2015 (green) and (ii) the magnitude-limited sample of OB stars presented by F2016 but here with only the O-type stars included. The shaded regions indicate bootstrapped 1σ estimates of the statistical significance of the variability in the τ distributions. The solid red line shows the expected τ distribution from a synthetic population drawn from a magnitude-limited sample (see discussion in F2016).

stars[6] from the complete distribution of known magnetic O-type stars we presented in Fig. 4 (reproduced here in Fig. 10 with a thin grey line).

(ii) We thus proceed here with the sample from F2016 as we use the change in radius, from current day to TAMS, that they determined with BONNSAI, for a direct comparison to their results (relevant values are listed in Table 1). The resulting distribution of expected field strengths at the TAMS for known magnetic O-type stars is shown in Fig. 10 (middle panel) as the leftmost thick pink histogram.

(iii) As we are attempting to determine whether we can rule out a detection bias, we here consider the most optimistic scenario in which stars with magnetic field values greater than or equal to the 68.3 per cent upper limit are likely to be detected. The 68.3 per cent upper limit distribution for the old O-type stars in the MiMeS sample is reproduced from the left-hand panel to the middle panel (blue thick histogram). This distribution overlaps with the distribution of expected field strengths at the TAMS for known magnetic O-type stars.

(iv) We now demonstrate how, in this optimistic scenario, the detectability of known magnetic stars at the TAMS also hinges on our level of confidence in the uncertainty of the estimated change of radius experienced by the known magnetic stars on their way to the TAMS.

To evolve the observed field strengths to the TAMS, we require an estimate of the current and TAMS radii of the stars. Fig. 11 shows the variation of radius as a function of fractional main-sequence age for a selection of models from the Brott et al. (2011) evolution tracks. A range of initial masses, spanning the range of masses for known magnetic O-type stars, are coloured according to the legend, and the rotation rates are bracketed between no rotation (in solid curves) and highest available rotation in the model grid, close to critical rotation (in dashed curves).

As can be seen from Fig. 11, the change in radius in the second half of the main sequence is very model dependent within a single set of evolutionary tracks. While most magnetic stars are currently slow rotators, it is unclear whether they began the MS as such, or whether they started the MS close to critical rotation and experienced the expected rapid magnetic braking (ud-Doula, Owocki & Townsend 2009). According to the models of Meynet, Eggenberger & Maeder (2011), these two scenarios would result in different interior structures. It is thus unclear which of the sets of non-magnetic models, if any, would be the most appropriate to describe magnetic evolution.

It may also be that the evolutionary tracks for stars with a strong fossil magnetic field are fundamentally different from those of non-magnetic stars due to the field interactions with the convection and angular momentum transport (e.g. Meynet et al. 2011; Petit et al. 2017; Keszthelyi et al. 2018). This could mean that (i) the radius evolution is different from that of non-magnetic stars (i.e. the stars stay more/less compact) and/or (ii) the real age and main-sequence lifetime of the magnetic star might be different from those implied by the non-magnetic evolutionary tracks.

Therefore, a systematic uncertainty in the ratio of radii of at least 50 per cent would certainly not be surprising. The shaded pink region in the middle panel of Fig. 10 represents a systematic uncertainty of 50 per cent in the radius increase for each known magnetic O-type star. Comparing the expected TAMS field strengths of known magnetic stars with the upper limits for stars near the end of their main-sequence lifetime, it is clear that not all stars would have been detected by the MiMeS survey, even if their TAMS radius is 50 per cent smaller than predicted.

Specific predictions for the rate at which older magnetic stars would have been detected by the MiMeS survey are therefore very dependent on the details of the evolution models used to predict the radius increase. This uncertainty in the radius increase would not have been too critical if the detection limits were, say, 10 times better, so that the thick blue histogram in the middle panel of Fig. 10 was located completely to the left of the pink shaded region.

We remind the reader that our comparison distribution corresponds to 68.3 per cent confidence, i.e. the optimistic assumption about detectability. While adopting the 95.4 per cent confidence

[6]NGC 1624-2, CPD-28 2561, Tr16-22, ζ Ori A.

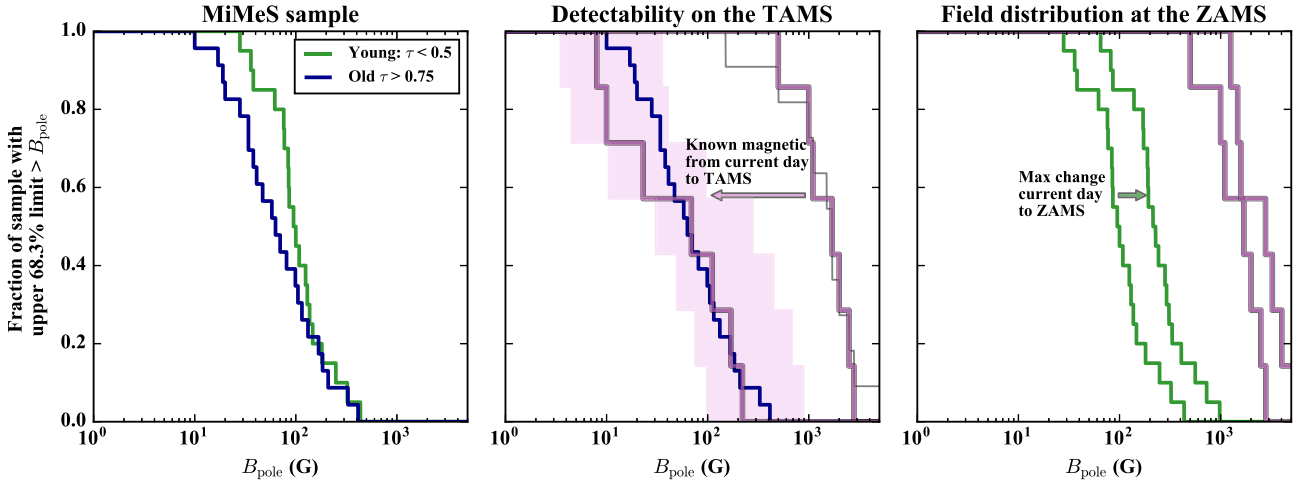

Figure 10. *Left*: Cumulative histogram of 68.3 per cent Stokes *V* upper limits for the M2015 sample (thick blue histogram of Fig. 8), separated into a young star sample ($\tau < 0.5$; thick green) and an old star sample ($\tau > 0.75$; thick blue). *Middle*: Comparison of the old sample (thick blue) with the field strength distribution of the known magnetic O-type stars included in the sample of F2016 (two thick pink histograms), evolving them from their current age values (right histogram) to their expected field strength at the TAMS (left histogram), assuming magnetic flux conservation. As the sample of F2016 only contained magnetic O-type stars with $V < 9$, we compare their current-day field strength distribution with the field strength distribution of all known magnetic O-type stars we used previously (thin grey histogram). The pink shaded region takes into account a systematic uncertainty of 50 per cent in the radius change between current age and TAMS. *Right*: Comparison between the field upper limits for the young star sample (leftmost green histogram) and the current-day magnetic field distribution of known magnetic O-type stars (leftmost, thick pink histogram). The rightmost green curve shows the maximum field these stars could have on the ZAMS, based on a maximum radius increase by a factor of 1.5. The rightmost pink curve shows the expected ZAMS distribution of field in known magnetic O-type stars based on the BONNSAI models of F2016.

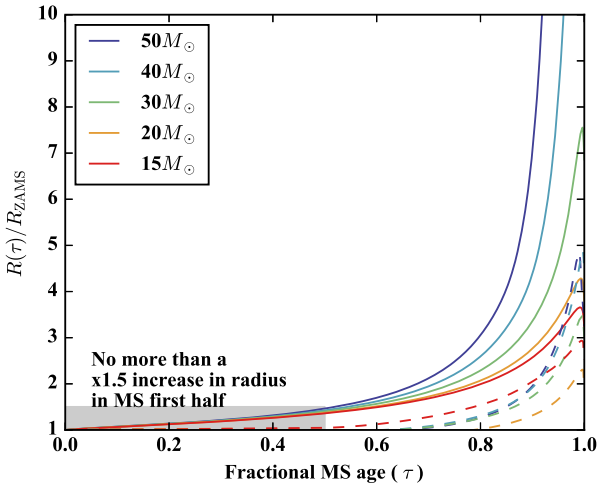

Figure 11. Variation of the radius as a function of the fractional main-sequence age for a selection of models from the Brott et al. (2011) evolution tracks. The initial rotation rates are bracketed between no rotation (in solid curves) and highest available rotation in the model grid, close to critical rotation (in dashed curves).

distribution (shifting the thick blue histogram to the right) relaxes the tension between the two distributions, our conclusions do not change: typical magnetic O-stars observed at the end of their MS evolution would have been difficult to detect with the precision achieved in the MiMeS survey.

We thus conclude that better upper limits, by at least a factor of 10, would be necessary for a clear and model-free exclusion of an observational bias to explain the apparent lack of old stars in the population of known magnetic O-type stars.

5.2 Magnetic desert

We now use our sample of upper limits to evaluate whether there is an extension of the 'magnetic desert' phenomenon for O-type stars. As discussed in Section 1.1, this so-called magnetic desert designates a feature in the distribution of field strengths of magnetic A and B stars, such that there are only a handful of known AB stars with detected fields of ∼100 G, even though the magnetic sensitivity for this type of stars is often at the 1–10 G level.

This magnetic desert in AB stars has an important diagnostic power both for stellar evolution models and for scenario for the origin of magnetism. Indeed, predicted 'initial *B*-field function' (IBF) combined with subsequent stellar evolution must result in an evolution of the surface magnetic field strength with time that prevents a long evolution phase at which the field would be below the magnetic desert cut-off but above the detection limit. Also, this magnetic desert implies that there are very few young magnetic AB stars born (or in the merger scenario have field generated) with a $\lesssim$100 G field, pointing towards a bimodality of the IBF.

In order to test whether the IBF of magnetic O-type stars might be bimodal, let us first consider the distribution of upper limits for the young subsample in the MiMeS survey we presented in the previous section as the green histogram in the left-hand panel of Fig. 10. This distribution is reproduced in the rightmost panel of Fig. 10.

Once again assuming that surface magnetic flux is conserved on stellar evolution time-scales, we can make a conservative estimate of the change of radius experienced by these stars since they were on the ZAMS by finding the maximum change in radius for an O-type star during the first half of the main sequence (we remind the reader that this corresponds to the maximum peak age of the young sample) for the set of evolution tracks already presented in Fig. 11. For all models, the maximum increase in radius is of a factor of 1.5.

Let us now imagine that all the stars in this young sample possess an undetected, current-day field with a dipolar value less than or equal to its upper limit. If each star could only have increased its radius by a factor of 1.5 at most since the ZAMS, then the ZAMS strength of this imaginary, undetected magnetic field could not have exceeded the current-day upper limit by more than a factor of 2.25 (or a shift of 0.35 dex in $\log(B_{\rm pole})$). This ZAMS upper limit distribution is represented by the rightmost green histogram in Fig. 10.

Comparing the lack of overlap between this ZAMS upper limit distribution and (i) the current-day distribution of field in known magnetic O-type stars (leftmost thick pink histogram) and (ii) the expected ZAMS distribution of fields in known magnetic O-type stars based on the BONNSAI models of F2016 (rightmost thick pink histogram), there is a good indication that the ZAMS IBF is bimodal: that young stars are expected to have either weak/absent magnetic fields or strong magnetic fields comparable to those of the known magnetic O-type stars. In other words, if a *large* fraction of young stars had magnetic fields with a strength of a few hundreds of gauss, evidence for these fields would be found in the MiMeS sample, as described in Section 4.1.

6 CONCLUSIONS

In this paper, we perform a statistical analysis of the MiMeS survey of O-type stars, to explore the dipolar field strengths allowed by the polarization spectra that lack any magnetic detection. We directly model the Stokes *V* profiles using Bayesian inference and adopting a dipolar topology.

We conclude that apart from the three magnetic candidate stars (HD 36486, HD 162978, HD 199579) identified by Grunhut et al. (2017) and the one additional magnetic candidate (HD 37468A) identified here, there is no strong evidence for a magnetic signal consistent with a dipolar field in any other individual star in our sample. We confirm that the six probable spurious detections identified by Grunhut et al. (2017) are indeed not compatible with a Stokes *V* signature arising from a dipolar magnetic field. The addition of one additional magnetic candidate does not change the magnetic field incidence of 7 ± 3 per cent reported by Grunhut et al. (2017) within the error bar.

We determine that if all the non-detected stars were hosting a magnetic field just below their detection limit, the distribution in strength of these undetected fields would be different from the distribution in strength of the known magnetic O-type stars.

Considering all of the target stars as a sample, we find a good correlation between the statistics obtained from the Stokes *V* profiles and the null profiles (which are nominally flat and expected to potential display only instrumental polarization or non-magnetic variability, if any). Using a Monte Carlo calculation, we also conclude that if all the stars in our sample were hosting a 100 G dipolar magnetic field, the direct detection rate would be rather low, only slightly higher than the observed bulk incidence of magnetism in massive stars. From this, we assess that the survey is nearly complete with respect to the detection of a lone magnetic star for dipolar field at the kilogauss level, and 50 per cent complete at the 250 G level. However, from a survey sample point of view, the aforementioned scenario (all stars hosting a magnetic field) would have resulted in statistically different odds ratio and credible region upper limit distributions obtained from Stokes *V* and from the null profiles.

We address two questions concerning the distribution of magnetic fields in O-type stars: (i) whether the 'magnetic desert' phenomenon extends to the O-type stars and (ii) whether the MiMeS sample of O-type star was able to systematically detect magnetic fields in old main-sequence O-type stars, and thereby constrain models of the evolution of their surface magnetism.

We find a good indication that the IBF is bimodal – young O-type stars are expected to have either weak/absent magnetic fields or strong magnetic fields.

We also find that better upper limits – better by at least a factor of 10 – would be necessary to affirm that the known magnetic O-type stars would have been unambiguously detected by the MiMeS Survey had they been on the TAMS. In other words, the current detection limits for the old stars in the MiMeS sample, combined with large uncertainties in the increase of the stellar radii over time in stellar evolution models, do not allow us to rule out a detection bias to explain the apparent lack of old magnetic O-type stars reported by F2016.

ACKNOWLEDGEMENTS

Based on MiMeS LP and archival spectropolarimetric observations obtained at the Canada–France–Hawaii Telescope, which is operated by the National Research Council of Canada, the Institut National des Sciences de l'Univers (INSU) of the Centre National de la Recherche Scientifique (CNRS) of France, and the University of Hawaii; on MiMeS LP and archival observations obtained using the Narval spectropolarimeter at the Observatoire du Pic du Midi (France), which is operated by CNRS/INSU and the University of Toulouse; and on MiMeS LP observations acquired using HARPSpol on the ESO 3.6 m telescope at La Silla Observatory, Program ID 187.D-0917. This research has made extensive use of the SIMBAD data base, operated at CDS, Strasbourg, France. We acknowledge the Canadian Astronomy Data Center (CADC). VP acknowledges support from the Fonds de Recherche du Quebec Nature et Technology (FQRNT), the ESO Scientific Visitor Programme. This material is based upon work supported by the National Science Foundation under grant no. 1747658. AD-U gratefully acknowledges the support of the Natural Science and Engineering Research Council of Canada (NSERC). The MiMeS collaboration acknowledges financial support from the Programme National de Physique Stellaire (PNPS) of INSU/CNRS. The authors would like to thank Dr. J. Grunhut for his contributions to the MiMeS project that made the work presented in this paper possible.

REFERENCES

Alecian E., Tkachenko A., Neiner C., Folsom C. P., Leroy B., 2016, A&A, 589, A47
Aurière M. et al., 2007, A&A, 475, 1053
Bagnuolo W. G., Jr., Riddle R. L., Gies D. R., Barry D. J., 2001, ApJ, 554, 362
Blazère A., Petit P., Neiner C. 2018, Contrib. Astron. Obs. Skalnate Pleso, 48, 48
Blazère A., Neiner C., Tkachenko A., Bouret J.-C., Rivinius T., 2015, A&A, 582, A110
Blazère A. et al., 2016, A&A, 586, A97
Borra E. F., Landstreet J. D., Mestel L., 1982, ARA&A, 20, 191
Briquet M. et al., 2012, MNRAS, 427, 483
Brott I. et al., 2011, A&A, 530, A115
Castro N. et al., 2015, A&A, 581, A81
Donati J.-F., Landstreet J. D., 2009, ARA&A, 47, 333
Donati J.-F., Semel M., Carter B. D., Rees D. E., Collier Cameron A., 1997, MNRAS, 291, 658

Fossati L. et al., 2015, A&A, 582, A45
Fossati L. et al., 2016, A&A, 592, A84 (F2016)
Georgy C., Meynet G., Ekström S., Wade G. A., Petit V., Keszthelyi Z., Hirschi R., 2017, A&A, 599, L5
Gregory P. C., 2005, ApJ, 631, 1198
Grunhut J. H. et al., 2017, MNRAS, 465, 2432
Hillier D. J., Miller D. L., 1998, ApJ, 496, 407
Hunter I., Lennon D. J., Dufton P. L., Trundle C., Simón-Díaz S., Smartt S. J., Ryans R. S. I., Evans C. J., 2008, A&A, 479, 541
Jeffreys H., 1998, Theory of Probability, 3rd edn. Oxford Univ. Press, Oxford
Keszthelyi Z., Wade G. A., Petit V., Meynet G., Georgy C., 2018, Contrib. Astron. Obs. Skalnate Pleso, 48, 124
Keszthelyi Z., Meynet G., Georgy C., Wade G. A., Petit V., David-Uraz A., 2019, MNRAS, 485, 5843
Landi degl'Innocenti E., Landolfi M., 2004, Astrophysics and Space Science Library, Vol. 307, Polarization in Spectral Lines. Kluwer, Dordrecht
Landstreet J. D. et al., 2008, A&A, 481, 465
Lignières F., Petit P., Aurière M., Wade G. A., Böhm T., 2014, in Petit P., Jardine M., Spruit H. C., eds, Proc. IAU Symp. 302, Magnetic Fields Throughout Stellar Evolution. Cambridge Univ. Press, Cambridge, p. 338
Maeder A., Meynet G., 2005, A&A, 440, 1041
Martins F. et al., 2015, A&A, 575, A34 (M2015)
Meynet G., Eggenberger P., Maeder A., 2011, A&A, 525, L11
Petit V., Wade G. A., 2012, MNRAS, 420, 773
Petit P. et al., 2010, A&A, 523, A41
Petit P. et al., 2011, A&A, 532, L13
Petit V. et al., 2013, MNRAS, 429, 398
Petit V. et al., 2017, MNRAS, 466, 1052
Rauw G., Sana H., Spano M., Gosset E., Mahy L., De Becker M., Eenens P., 2012, A&A, 542, A95
Salpeter E. E., 1955, ApJ, 121, 161
Schneider F. R. N., Langer N., de Koter A., Brott I., Izzard R. G., Lau H. H. B., 2014, A&A, 570, A66
Schneider F. R. N., Podsiadlowski P., Langer N., Castro N., Fossati L., 2016, MNRAS, 457, 2355
Schneider F. R. N., Castro N., Fossati L., Langer N., de Koter A., 2017, A&A, 598, A60
Shultz M. E. et al., 2018, MNRAS, 475, 5144
Stickland D. J., Pike C. D., Lloyd C., Howarth I. D., 1987, A&A, 184, 185
ud-Doula A., Owocki S. P., Townsend R. H. D., 2009, MNRAS, 392, 1022
Wade G. A. et al., 2016, MNRAS, 456, 2
Walborn N. R., 1972, AJ, 77, 312

APPENDIX A: LINE PROFILE MODELS FOR SB2 SYSTEMS

In this appendix, we illustrate the intensity model fit for the SB2 system to provide a reference for the primary and secondary designation adopted (Fig. A1).

For HD 37043, our single LSD profile yields various possible equivalent width (EW) ratios for the primary and secondary, all compatible with the results of Stickland et al. (1987) and Bagnuolo et al. (2001). We opt for a solution with a smaller EW for the primary than presented in Paper I – this yields a more conservative estimate of the field upper limits.

As discussed in Paper I, our LSD profiles for the SB2 HD 164794 (9 Sgr) do not show two components. However, the line characteristics have been well constrained by Rauw et al. (2012), so we here use their broadening value and radial velocity solution to fit our profiles.

In Paper I, HD 191201 is listed as an O + O system, but is given a spectral type of O9.5 III + B0 IV. We include the secondary star in our sample.

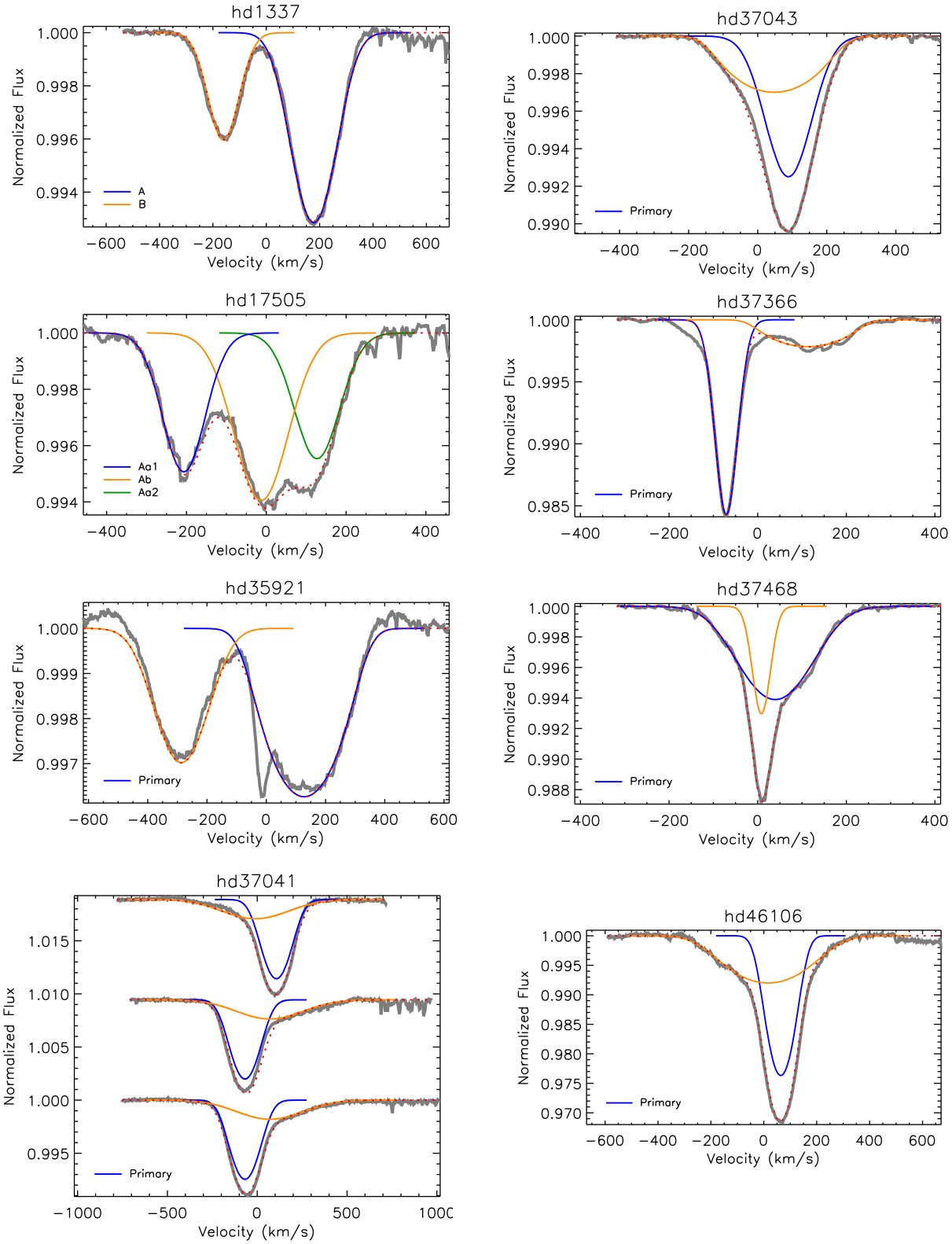

Figure A1. Illustration of model fit for the SB2 systems in the sample. The primary and secondary designation matches those of Table 2.

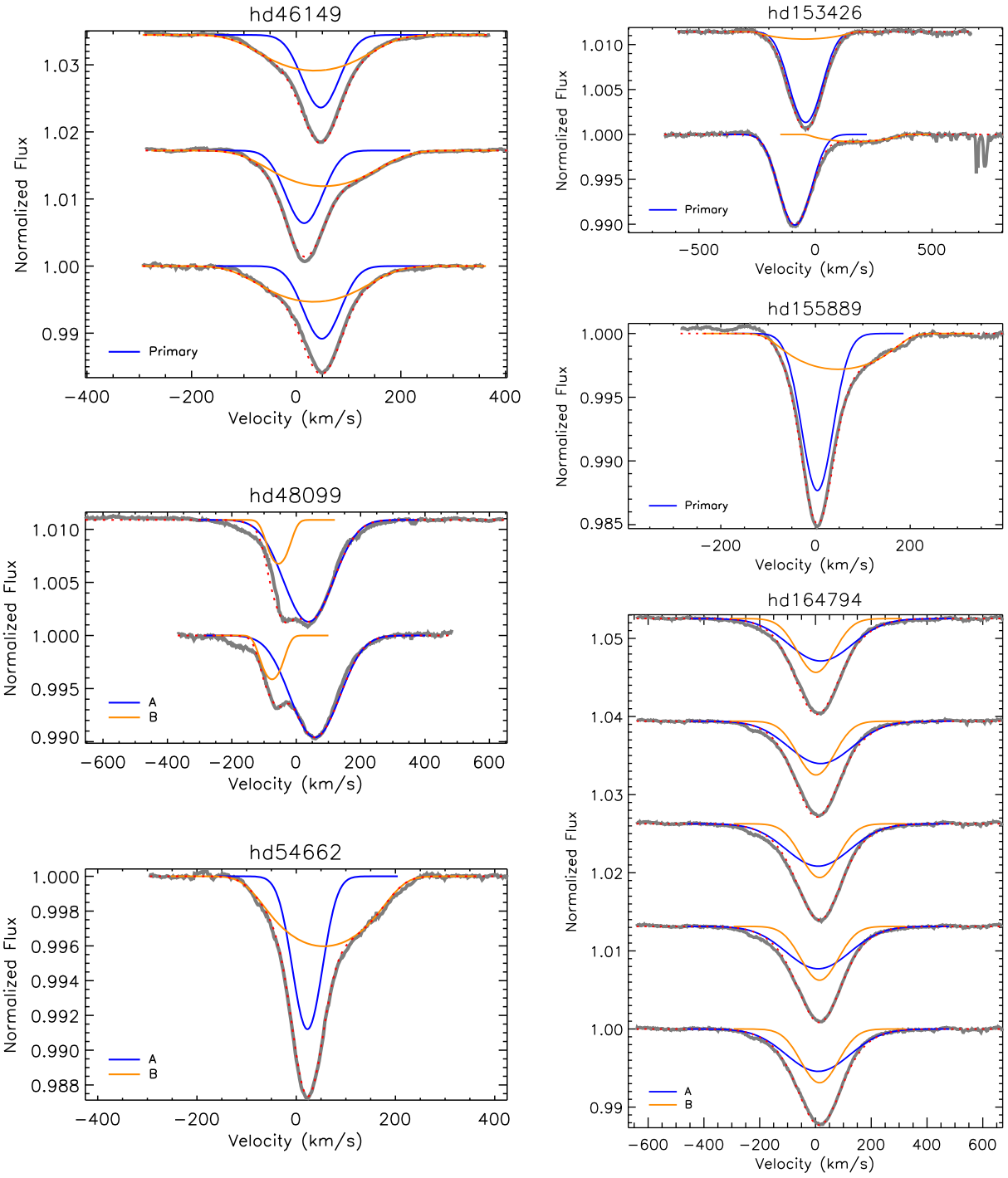

Figure A1 – *continued*

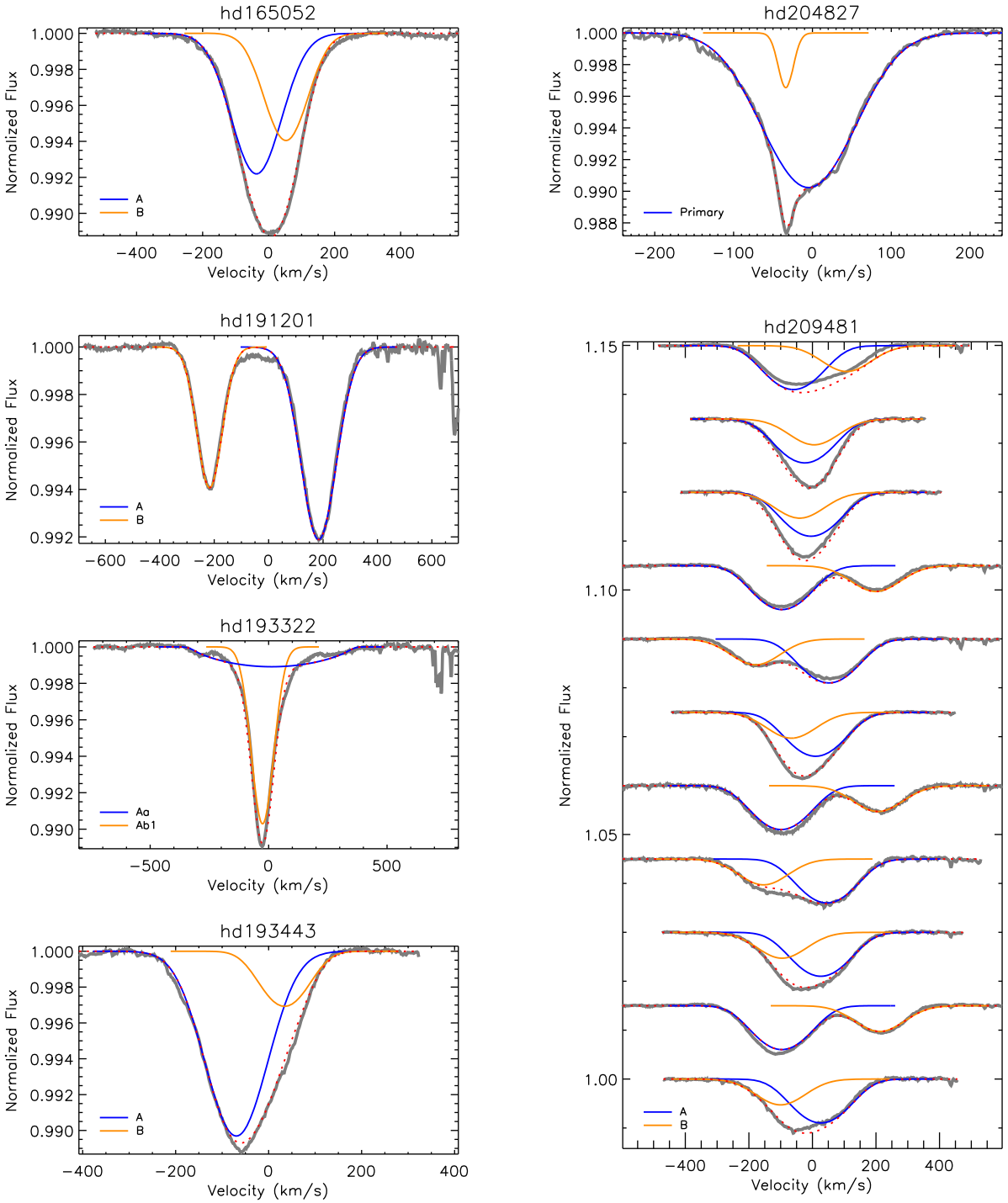

Figure A1 – *continued*

This paper has been typeset from a TEX/LATEX file prepared by the author.